PLOS PATHOGENS

RESEARCH ARTICLE

NS5A domain I antagonises PKR to facilitate the assembly of infectious hepatitis C virus particles

Shucheng Chen, Mark Harris*

School of Molecular and Cellular Biology, Faculty of Biological Sciences and Astbury Centre for Structural Molecular Biology, University of Leeds, Leeds, United Kingdom

* m.harris@leeds.ac.uk

Citation: Chen S, Harris M (2023) NS5A domain I antagonises PKR to facilitate the assembly of infectious hepatitis C virus particles. PLoS Pathog 19(2): e1010812. https://doi.org/10.1371/journal.ppat.1010812

Editor: Glenn Randall, The University of Chicago, UNITED STATES

Received: August 18, 2022

Accepted: February 2, 2023

Published: February 16, 2023

Data Availability Statement: All relevant data are within the manuscript and its Supporting Information files.

Funding: This work was supported by a Wellcome Investigator Award (grant number 096670), and an MRC project grant (MR/S001026/1) to MH. SC was supported by a University of Leeds/China Scholarship Council PhD studentship. The funders had no role in study design, data collection and analysis, decision to publish, or preparation of the manuscript.

Abstract

Hepatitis C virus NS5A is a multifunctional phosphoprotein comprised of three domains (DI, DII and DIII). DI and DII have been shown to function in genome replication, whereas DIII has a role in virus assembly. We previously demonstrated that DI in genotype 2a (JFH1) also plays a role in virus assembly, exemplified by the P145A mutant which blocked infectious virus production. Here we extend this analysis to identify two other conserved and surface exposed residues proximal to P145 (C142 and E191) that exhibited no defect in genome replication but impaired virus production. Further analysis revealed changes in the abundance of dsRNA, the size and distribution of lipid droplets (LD) and the co-localisation between NS5A and LDs in cells infected with these mutants, compared to wildtype. In parallel, to investigate the mechanism(s) underpinning this role of DI, we assessed the involvement of the interferon-induced double-stranded RNA-dependent protein kinase (PKR). In PKR-silenced cells, C142A and E191A exhibited levels of infectious virus production, LD size and co-localisation between NS5A and LD that were indistinguishable from wildtype. Co-immunoprecipitation and in vitro pulldown experiments confirmed that wildtype NS5A domain I (but not C142A or E191A) interacted with PKR. We further showed that the assembly phenotype of C142A and E191A was restored by ablation of interferon regulatory factor-1 (IRF1), a downstream effector of PKR. These data suggest a novel interaction between NS5A DI and PKR that functions to evade an antiviral pathway that blocks virus assembly through IRF1.

Author summary

The non-structural 5A protein (NS5A) of hepatitis C virus (HCV) plays a critical role in both virus genome replication and the assembly of infectious virus particles. NS5A is a target for potent and highly efficacious direct acting antivirals used extensively for HCV treatment. NS5A comprises 3 domains. Here, we show that the N-terminal domain I (DI) plays a role in virus assembly. Mutations in DI block both virus assembly and the perturbation of lipid droplet morphology that is a hallmark of HCV infection. Strikingly, this phenotype is abrogated by silencing of the cellular cytoplasmic double-stranded RNA

Competing interests: The authors have declared that no competing interests exist.

sensor, PKR, a key antiviral factor. These mutations have therefore uncovered a hitherto uncharacterised antiviral pathway controlled by PKR which functions to block assembly of infectious virus particles.

Introduction

Hepatitis C Virus (HCV) is an enveloped virus in the Flaviviridae family with a positive-sense, single-stranded RNA genome [1]. HCV infection is a globally prevalent public health problem, it is the leading causative agent of chronic liver diseases including cirrhosis, hepatocellular carcinoma (HCC) and liver cancer [2,3]. As of 2015, approximately 71 million individuals worldwide (1% of the global population) were estimated to be chronically infected with HCV, resulting in more than 390,000 deaths per annum from cirrhosis and HCC [4]. The recent introduction of direct-acting antivirals (DAAs), small molecule inhibitors of virus genome replication, has dramatically changed the clinical landscape. DAA treatment is able to cure the majority (~99%) of patients rapidly and with no side-effects [5].

The HCV RNA genome contains approximately 9600 nucleotides and is comprised of a 5′-untranslated region (UTR), a single open reading frame (ORF) encoding a single polyprotein of 3000 amino acids, and a 3′-UTR [6,7]. The polyprotein is processed co- and post-translationally by cellular and viral proteases into 10 viral proteins, namely the structural proteins: Core, E1 and E2, and p7, and the non-structural proteins: NS2, NS3, NS4A, NS4B, NS5A and NS5B [8].

The subject of this study, NS5A, is a RNA-binding phosphoprotein with a calculated molecular mass of 49 kDa, comprised of an N-terminal amphipathic α-helix (residues 1–33) that anchors the protein to cytoplasmic membranes, a structured domain 1 (DI), and two intrinsically disordered domains (DII and DIII) linked by two low-complexity sequences (LCS-1 and -2) [9–11] (Fig 1A). X-ray crystallography demonstrated that NS5A DI is a highly structured zinc-binding domain. In addition, four different conformations of DI from genotype 1a and 1b were observed, with the same monomeric unit but exhibiting different dimeric arrangements [12–14]. NS5A DI was considered to be required exclusively for genome replication [11], however, our previous work revealed that DI was also involved in assembly of infectious virus [15]. Notably, NS5A DI has been identified as the target for one class of DAAs (eg daclatasvir and velpatasvir), as judged by the fact that mutations in DI result in resistance to these DAAs. Although the mode of action of these DAAs is not understood, they inhibit virus replication with extraordinary potency (pM EC_{50} values in culture) and have been shown to independently block both virus genome replication and virus assembly with different kinetics [16], providing further support for the role of DI in virus assembly. In contrast to DII and DIII, DI exhibits high sequence homology across all hepaciviruses [17–20], indicating critical and conserved functions in the virus life cycle.

NS5A plays a variety of roles in the HCV life cycle. With the other non-structural proteins (NS3 to NS5B) it constitutes the viral replicase which, together with cellular factors, remodels the ER membrane to form viral replication organelles termed the membranous web (MW) [21–24]. NS5A binds directly to viral RNA [25,26], but also modulates HCV RNA replication by interacting with other NS proteins and various cellular factors, such as vesicle-associated membrane protein-associated proteins A and B (VAP-A, VAP-B), cyclophilin A (CypA) and phosphatidylinositol-4-kinase IIIα (PI4KIIIα) [27–32].

NS5A plays an additional role in the assembly of infectious virus particles. NS5A interacts with Core [33] and both proteins are recruited to lipid droplets (LD). If this targeting is blocked either genetically or pharmacologically virus assembly is inhibited, suggesting that

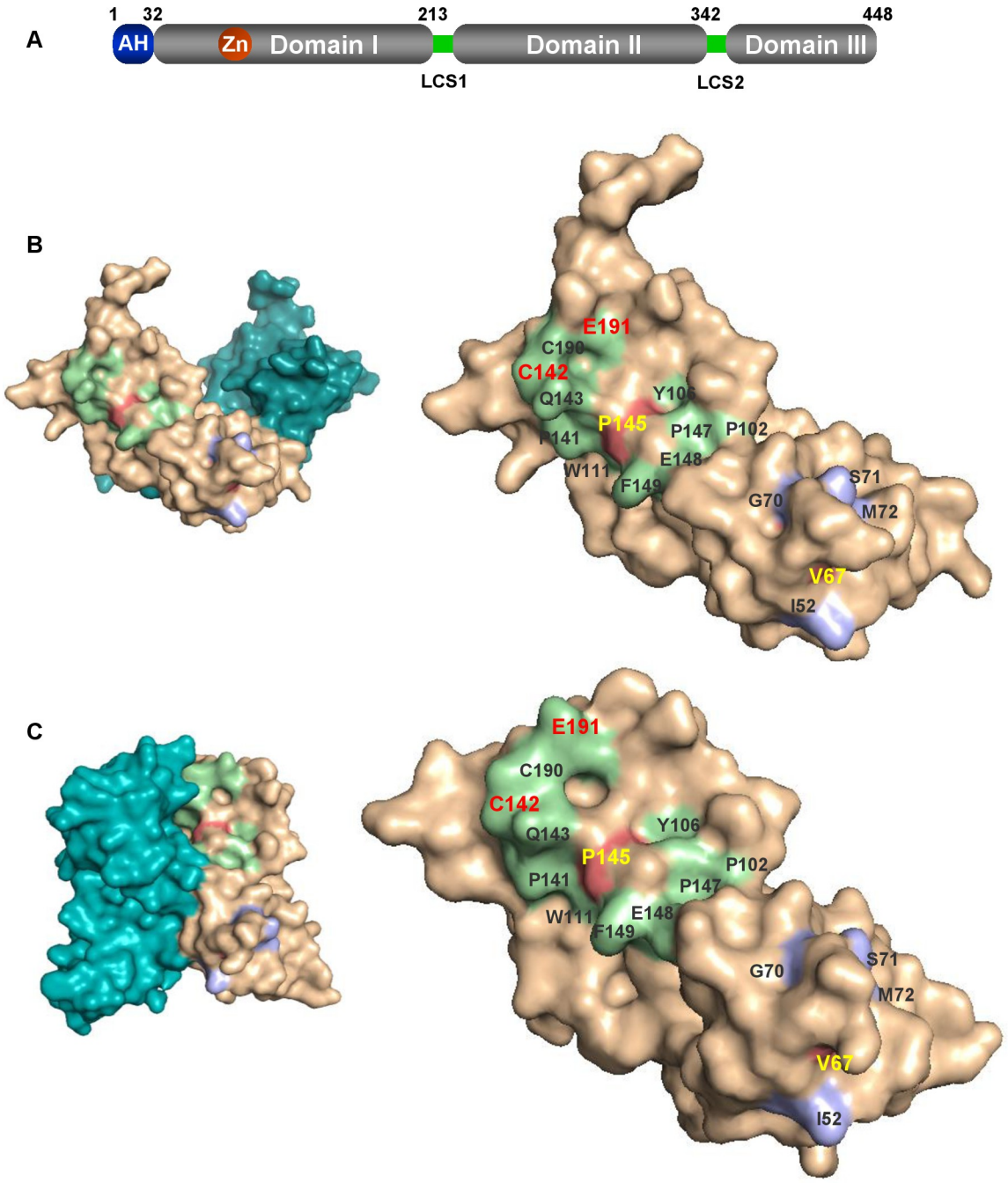

Fig 1. Location of mutated residues in DI. (A) Structure of NS5A illustrating the three domains. AH: amphipathic helix (blue), LCS: low complexity sequence (green). **(B, C)** Conserved and surface exposed residues proximal to V67 (blue) and P145 (green) are displayed in the two NS5A DI (genotype 1b) structures 1ZH1 **(B)** and 3FQM **(C)**. Dimeric forms are shown on the left, with the monomers on the right.

https://doi.org/10.1371/journal.ppat.1010812.g001

LDs provide a platform for virion formation [34]. NS5A interacts with a number of cellular proteins that play a critical role in the assembly process. These include: diacylglycerol acyltransferase 1 (DGAT1), oxysterol binding protein (OSBP), phosphatidylserine-specific phospholipase A1 (PLA1A), Rab18, Tail-Interacting Protein 47 (TIP47) and Annexin A3 [35–40].

However, for both genome replication and virus assembly, the precise molecular mechanisms underpinning the roles of NS5A remain elusive.

Double-stranded RNA (dsRNA)-dependent protein kinase (PKR) acts as both a sensor of virus infection by binding to viral dsRNA resulting in its activation, and also an effector via downstream consequences such as inhibition of protein translation and induction of apoptosis [41]. NS5A has been reported to interact with PKR via a region in DII that includes the interferon-sensitivity determining region (ISDR), the sequence of which correlates with the sensitivity of virus isolates to interferon treatment, and a further 26 residues C-terminal to the ISDR [42]. This interaction blocks PKR activation [43]. Multiple mechanisms by which PKR inhibits the HCV lifecycle have been proposed: inhibition of PKR has been shown to promote HCV genome replication and translation [44], in contrast HCV has also been reported to recruit and activate PKR to trigger induction of interferon stimulated genes (ISGs) [45,46]. Once activated, PKR has a number of downstream effects: the best characterised is the phosphorylation of the α subunit of eukaryotic initiation factor 2 (eIF2α) at Ser51 [47,48]. This blocks cap-dependent translation by preventing recycling of eIF2 to the initiation complex [49]. PKR also activates the transcription factor NF-κB independently of PKR catalytic activity [50,51]. PKR activation leads to dissociation of the inhibitor IκB from the p50/p65 NF-κB complex, which then enters the nucleus and activates transcription [52,53]. IFN regulatory factor 1 (IRF1) is also activated by PKR, and IRF1 activation by exogenous dsRNA was reported to be blocked by binding of the NS5A ISDR to PKR [54].

In this study, we confirmed the role of NS5A DI in HCV assembly. We identified two surface-exposed and conserved residues, which were not essential for virus genome replication, but disrupted the production of infectious virus particles. LD formation and the co-localisation between Core, NS5A and LDs were disrupted in cells infected with these two mutants. Intriguingly, silencing of PKR rescued the production of infectious virus, LD size and co-localisation with Core and NS5A for these two mutants. Silencing of the downstream factor IRF1 also rescued production of infectious virus. These data reveal that NS5A DI functions to allow HCV to evade inhibition of virus assembly by PKR and IRF1, and uncovers a hitherto unidentified function of PKR to inhibit virus assembly.

Results

Genome replication phenotypes of residues proximal to V67 and P145

NS5A DI was thought to function exclusively in HCV genome replication [11] until several years ago when we challenged this dogma and demonstrated that NS5A DI in HCV genotype 2a (JFH-1) also plays a critical role in virus assembly [15]. This was exemplified by the phenotype of alanine substitutions at V67 and P145: in Huh7 cells these mutants exhibited a significant RNA replication defect. However, in Huh7.5 cells which have a defective innate immune response to HCV as a result of a dominant negative RIG-I mutation [55], these mutants exhibited a comparable level of RNA replication to wildtype, but blocked production of infectious virus particles [15]. To investigate whether the V67A/P145A phenotype was unique we identified a panel of fifteen surface-exposed residues proximal to V67 and P145 that are highly conserved across all HCV genotypes, shown in Fig 1B and 1C and highlighted on the monomer structures of genotype 1b NS5A DI (PDB 1ZH1 and 3FQM) [12,14]. These residues were substituted by alanine in the context of a JFH-1 derived sub-genomic replicon (mSGR-luc-JFH-1) which contains unique restriction sites flanking the NS5A coding sequence, and a firefly luciferase reporter [56]. An NS5B GND mutant (polymerase-inactive) was used as a negative control [57]. As shown in S1 Fig these mutants exhibited a number of phenotypes: Five residues proximal to V67 (I52, G70 and M72), or P145 (P141 and E148) exhibited the same

phenotype as V67, ie reduced replication in Huh7 cells, which was restored to wildtype (WT) levels in Huh7.5. In Huh7 cells these mutants showed a reduction in luciferase levels at 24 hpe, only recovering to the 4 hpe input values by 72 hpe, consistent with a severe replication defect (compared to WT which exhibited a 27-fold increase in luciferase values from 4–48 hpe). In Huh7.5 cells these mutants were indistinguishable from wildtype, exhibiting between 25-45-fold increase in luciferase values from 4–72 hpe. Six residues proximal to V67 (S71), or P145 (C142, Q143, P147, C190 and E191), were dispensable for genome replication in either Huh7 or Huh7.5 cells, showing levels of replication that were indistinguishable from wildtype in both cell lines. In contrast, four residues proximal to P145 (P102, Y106, W111 and F149) were absolutely required for genome replication in both cell lines and were thus excluded from further analysis in this study.

C142 and E191 are required for virus assembly

We next investigated whether the eleven residues that were partially or completely dispensable for genome replication played a role in virus assembly and release. Alanine substitution of all of these residues were generated in the full-length mJFH-1 infectious clone [56]. The assembly phenotype of these mutants was evaluated in Huh7.5 cells as none of these mutants exhibited a replication phenotype in these cells, allowing us to interrogate effects on assembly in the absence of confounding factors resulting from a replication defect. In addition Huh7.5 cells supported higher levels of virus genome replication (S1 Fig–compare WT values in A and B). As shown in S2 Fig, nine of these mutants produced similar levels of released infectious virus to WT, however two of the mutants (C142A and E191A) exhibited a significant defect in virus production. We therefore focused our further investigations on these two mutants. Of note, these two mutants exhibited a different phenotype from the original P145A mutant as they had no replication defect in either Huh7 or Huh7.5 cells. Interestingly, C142 was shown to form a disulphide bond with C190 in the 'open' dimer conformation (1ZH1), but not the 'closed' dimer (3FQM) of NS5A DI (S3 Fig). Previous mutagenesis had shown that this disulphide bond is not required for genome replication [11], consistent with our replication data (S1 Fig). As C190 is positioned between C142 and E191 on the NS5A DI surface (S3 Fig), we included C190A as a control in the detailed analysis of the C142A and E191A phenotypes, as described henceforth.

We first confirmed virus genome replication for the mutant infectious clones C142A, C190A and E191A both directly by qPT-PCR (Fig 2A), and indirectly by quantifying NS5A positive cells using an IncuCyte S3 cell imager [58] (Fig 2B). Reassuringly, replication of all three mutants was indistinguishable from WT, mirroring the SGR data. Western blot analysis confirmed that NS5A and the structural proteins Core and E2 were expressed at equivalent levels to WT (Fig 2C).

To assess both virus assembly and release we proceeded to determine intracellular and extracellular virus titres (Fig 2D). This analysis revealed that C142 was absolutely required for virus assembly with levels of both intracellular and extracellular virus indistinguishable from the negative control (NS5B GND). In contrast, C190A had no effect on WT levels of infectivity, and E191A exhibited an intermediate phenotype with an approximately 2-log reduction compared to WT. We conclude that C142 and E191 play a role in virus assembly, and the fact that C190 is dispensable further suggests that the disulphide bond observed in the 'open' structure of DI is not required for the function of NS5A during genome replication or assembly.

NS5A DI mutants alter the morphology and distribution of lipid droplets

To better characterise the role of C142 and E191 on infectious virus production, we used high resolution confocal microscopy (Airyscan) to observe the co-localisation between viral

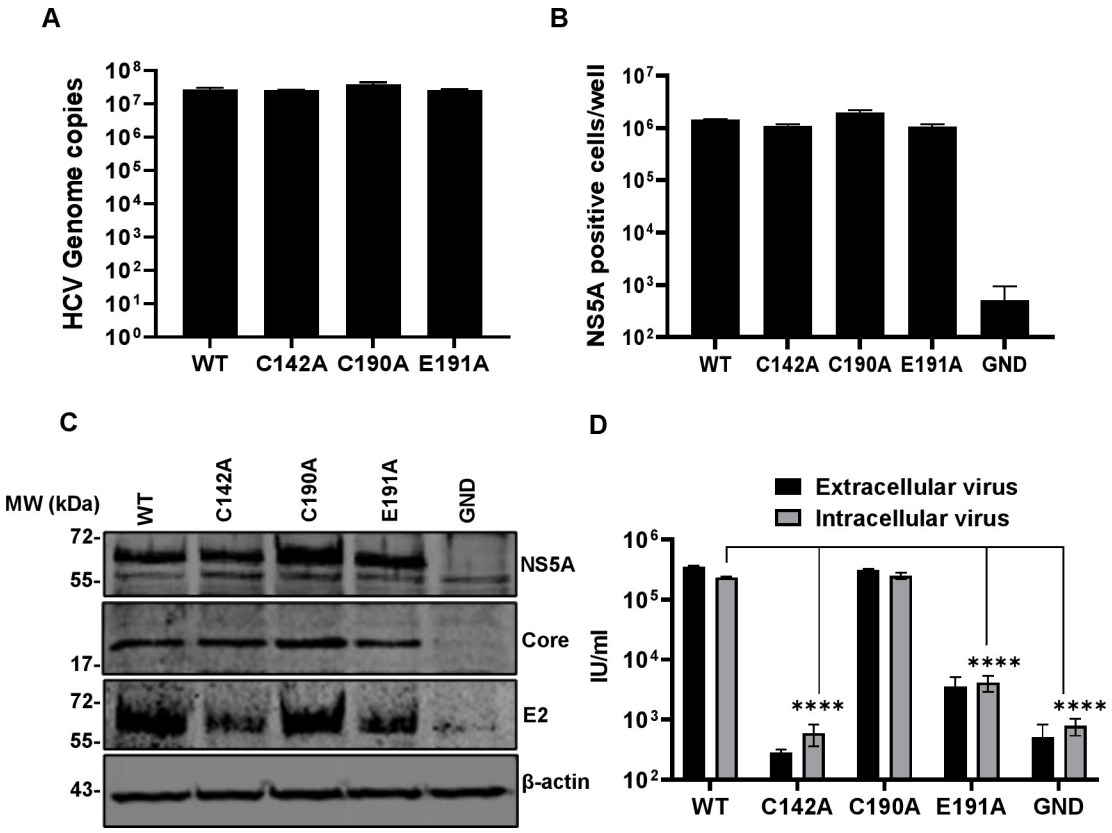

Fig 2. Virus assembly phenotypes in Huh7.5 cells. Huh7.5 cells were electroporated with mJFH-1 WT and DI mutant C142A, C190A and E191A RNAs, together with an NS5B GND mutant as negative control. Virus genome replication was analysed directly by quantification of genome copies in cell lysates using qRT-PCR, data shown have the GND values subtracted (**A**), and indirectly by enumerating NS5A positive cells at 72 hpe using the IncuCyte S3 (**B**). (**C**) Cell lysates were collected at 72 hpe and analysed by western blotting with the indicated antibodies. (**D**). Extra- and intracellular virus harvested at 72 hpe were titrated in Huh7.5 cells and quantified using the IncuCyte S3. N = 3, significant differences from WT denoted by **** ($P<0.0001$).

https://doi.org/10.1371/journal.ppat.1010812.g002

proteins and cellular factors. Key organelles during virus assembly are lipid droplets (LDs), to which both Core [59] and NS5A [60] are recruited. The disruption of LDs either pharmacologically or genetically [61] inhibits virus assembly. We previously showed that in cells infected with the P145A mutant virus, LDs were more abundant and smaller in size compared to WT infected cells [15]. As shown in Fig 3 (and quantitatively analysed in Fig 4), this phenotype was recapitulated for both C142A and E191A: cells infected with WT and C190A exhibited an average of 100 LD with a cross-sectional area of approximately 1.0 μm^2, whereas C142A and E191A displayed >200 LD with a significantly smaller area (0.2 μm^2), similar to mock-infected cells (Fig 4A).

The differences in both LD size and quantity were consistent with the assembly defective phenotypes of C142A and E191A. To extend this analysis we quantified the colocalisation of Core and NS5A with LDs. As shown in Fig 4B, the percentage of NS5A co-localising with LDs (grey boxes) was significantly decreased for C142A and E191A compared to WT. However, the inverse value (percentage of LD colocalised with NS5A –red boxes) was comparable for all mutants and WT, consistent with the suggestion that the interaction of NS5A with LD was disrupted by C142A and E191A mutations. Similar results were observed for the interaction of LD with Core (Fig 4C). Finally, we quantified the colocalisation of Core and NS5A and observed a reduction for C142A and E191A (Fig 4D). This reduction was less pronounced for

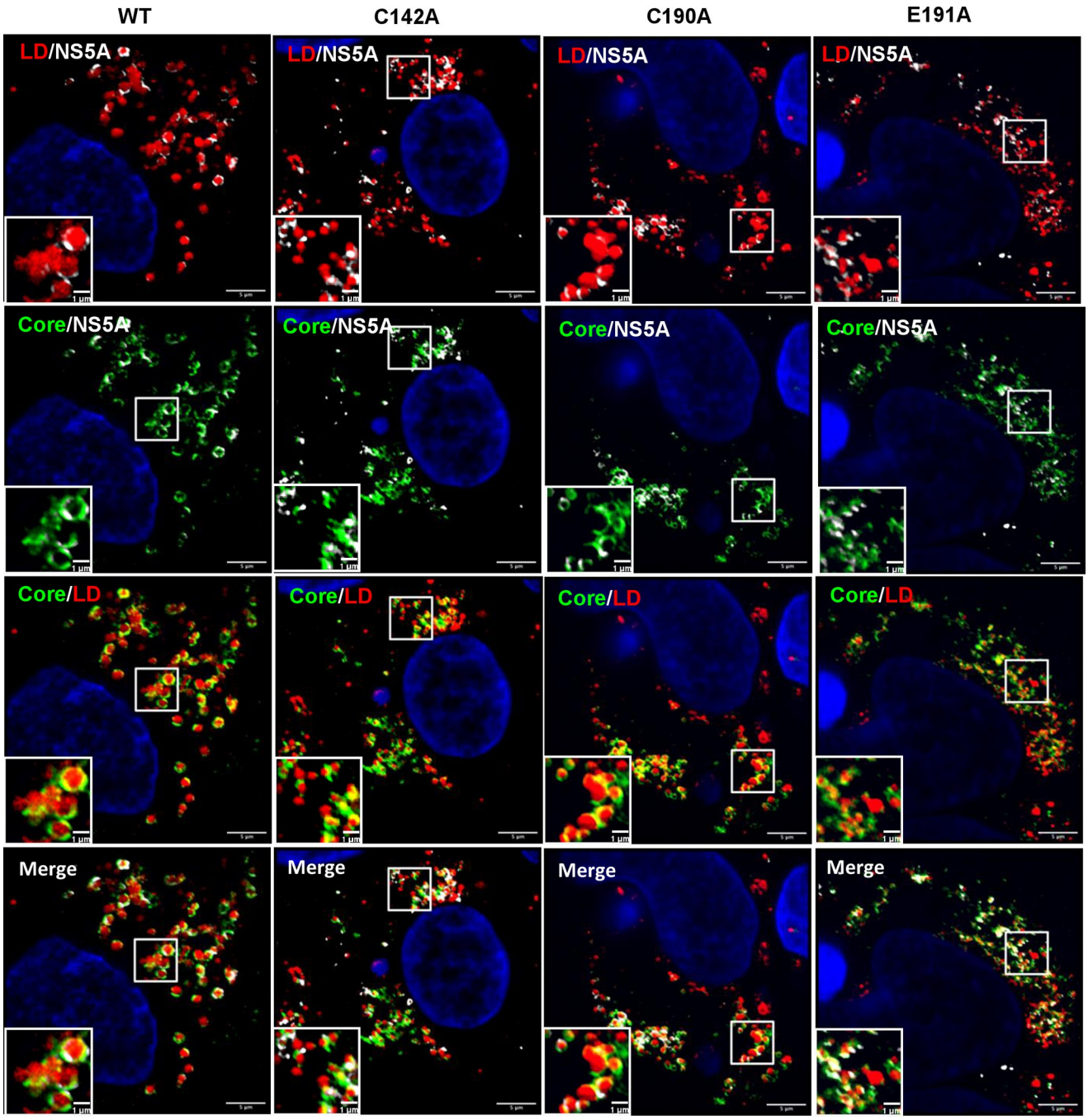

Fig 3. Co-localisation between NS5A, Core and LD. Huh7.5 cells were electroporated with mJFH-1 WT and DI mutant C142A, C190A and E191A RNAs and seeded on to coverslips. At 72 hpe cells were stained with sheep anti-NS5A (white), rabbit anti-Core (green), BODIPY 558/568-C12 (red) and DAPI. Co-localisation was observed using Airyscan microscopy. Representative images are presented. A representative image of mock electroporated cells is shown in S6A Fig. Scale bars are 5 μm and 1 μm (insets).

https://doi.org/10.1371/journal.ppat.1010812.g003

E191A, consistent with the less marked phenotype of this mutant. We also assessed the distribution of LDs by quantifying their distance from the nucleus. As shown in the representative images in Fig 5A, and quantified in Fig 5B, LDs in C142A and E191A infected cells were significantly closer to the nucleus than WT or C190A, although still more dispersed than mock

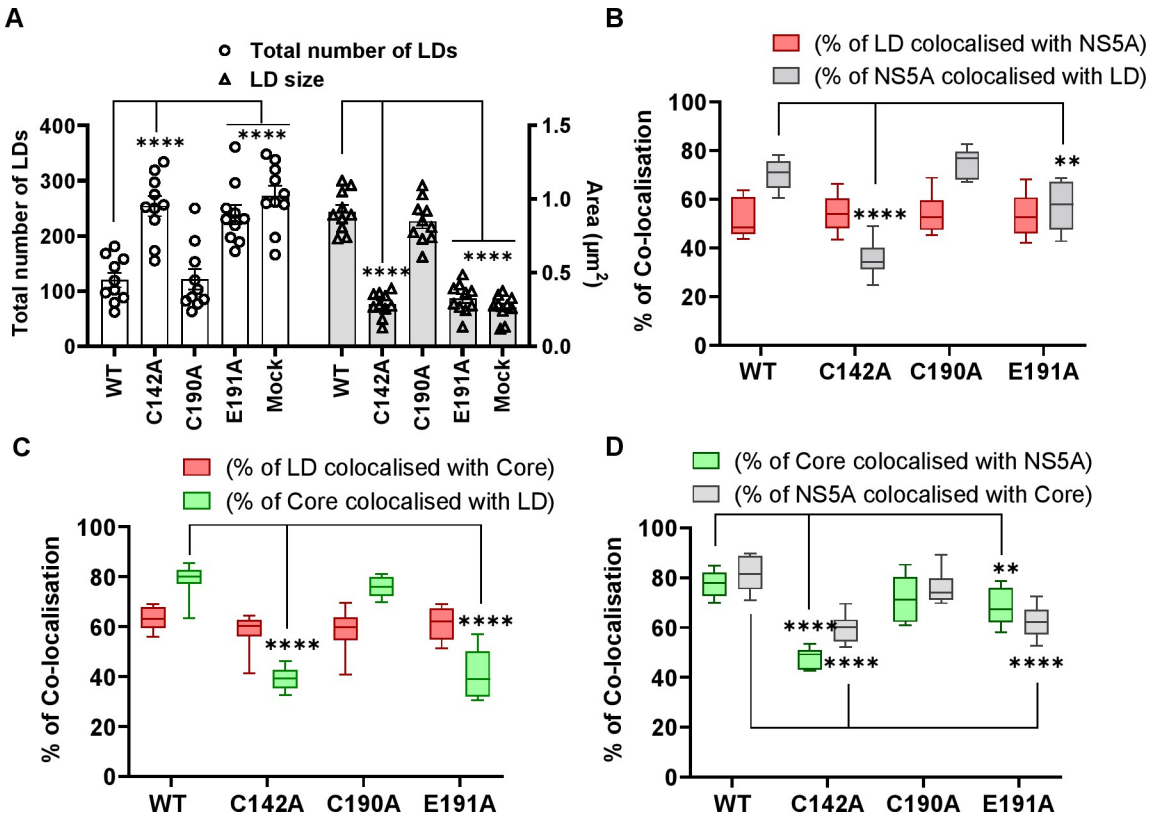

Fig 4. Quantification of LD size and co-localisation with NS5A and Core. (A) LD numbers and size in cells from Fig 3 were calculated using Analyze Particles module of Fiji. Mock: uninfected Huh7.5 cells. 10 cells were analysed for each sample. **(B)** Quantification of the percentage of LD colocalized with NS5A (red), and NS5A colocalized with LD (grey). **(C)** Quantification of the percentage of LDs colocalized with Core (red), and Core colocalized with LD (green). **(D)** Quantification of the percentage of Core colocalized with NS5A (green), and NS5A colocalized with Core (grey). Co-localisation was analyzed in 10 cells for each construct using Fiji. Significant differences from WT denoted by ** ($P<0.01$) and **** ($P<0.0001$).

https://doi.org/10.1371/journal.ppat.1010812.g004

infected cells. Together, these data are consistent with the proposition that NS5A DI is involved in the targeting of NS5A to LDs and functions to perturb LD morphology and distribution to promote virus assembly.

PKR silencing or inhibition recovers the virus assembly phenotype of C142A and E191A

We sought to further investigate the mechanism underpinning the role of NS5A DI in virus assembly. Given that we, and others, had previously shown that NS5A binds viral RNA [25,26], we considered that NS5A might be involved in transporting nascent genomic RNA from replication sites to assembly sites via LD [62] where NS5A could deliver the RNA to the Core protein. Core would then transport the RNA to the site of virion assembly. One potential consequence of this process is that the RNA would be transiently exposed in the cytosol, permitting detection by innate cytosolic sensors such as PKR. This prompted us to investigate whether silencing of PKR might restore the assembly phenotype of C142A and E191A.

We generated a stable Huh7.5 cell line in which expression of PKR was silenced using a lentivirus delivered CRISPR/Cas9 construct [63] (Fig 6A) and proceeded to analyse the genome replication and assembly of the 3 DI mutants in these PKR silenced Huh7.5 cells. As expected, both genome replication (Fig 6B) and viral protein production (Fig 6C and 6D) were

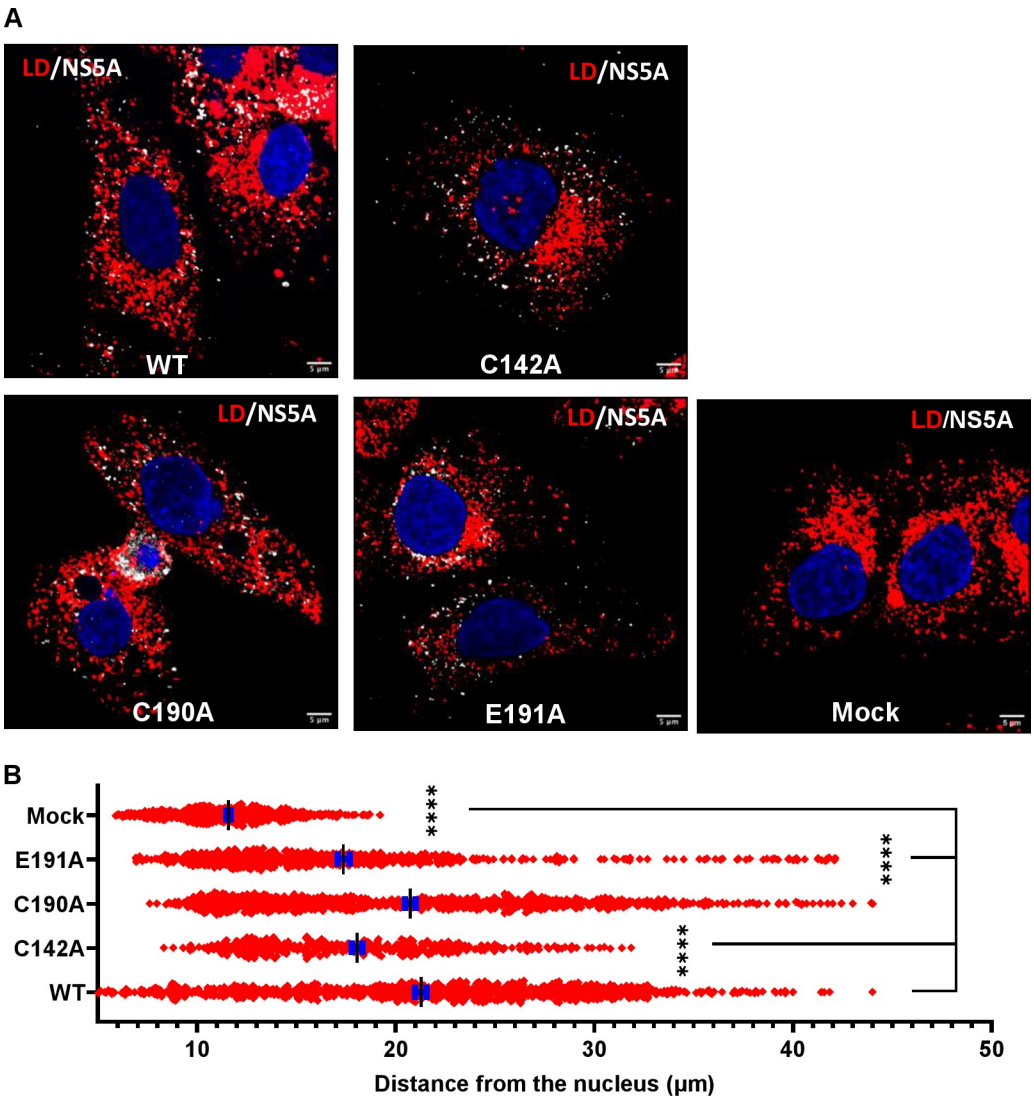

Fig 5. Analysis of LD distribution. (A) Cells were stained at 72 hpe with sheep anti-NS5A (white), BODIPY 558/568-C12 (red) and DAPI. **(B)** Distances of LDs from the nuclear membrane were evaluated using the Analyze Particles module of Fiji. 10 cells were analysed for each sample. Significant differences from WT denoted by **** ($P<0.0001$).

https://doi.org/10.1371/journal.ppat.1010812.g005

unaffected by the absence of PKR. Indeed, overall levels of genome replication as measured by qRT-PCR modestly increased (3-fold) compared to Huh7.5 cells (compare Fig 6B to Fig 2A). A surprising picture emerged when we analysed the assembly and release of the mutants: production of infectious virus by C142A and E191A was restored to the same level as WT and C190A in PKR silenced Huh7.5 cells (Fig 6E). To confirm that this was due to the lack of PKR, as opposed to an off-target effect of the sgRNA, we treated Huh7.5 cells with the small molecule PKR inhibitor C16 (1 μM), a concentration shown to inhibit PKR phosphorylation in Huh7 cells whilst still allowing cell growth [64], at 24 h post electroporation. Reassuringly, pharmacological inhibition of PKR function also restored the production of infectious virus by C142A and E191A (Fig 6F). To further confirm the direct role of PKR, we exogenously overexpressed PKR in the silenced Huh7.5 cells (Fig 6A), prior to analysing release of infectious WT and mutant viruses. As shown in Fig 6G, this resulted in a reduction in titres of C142A and

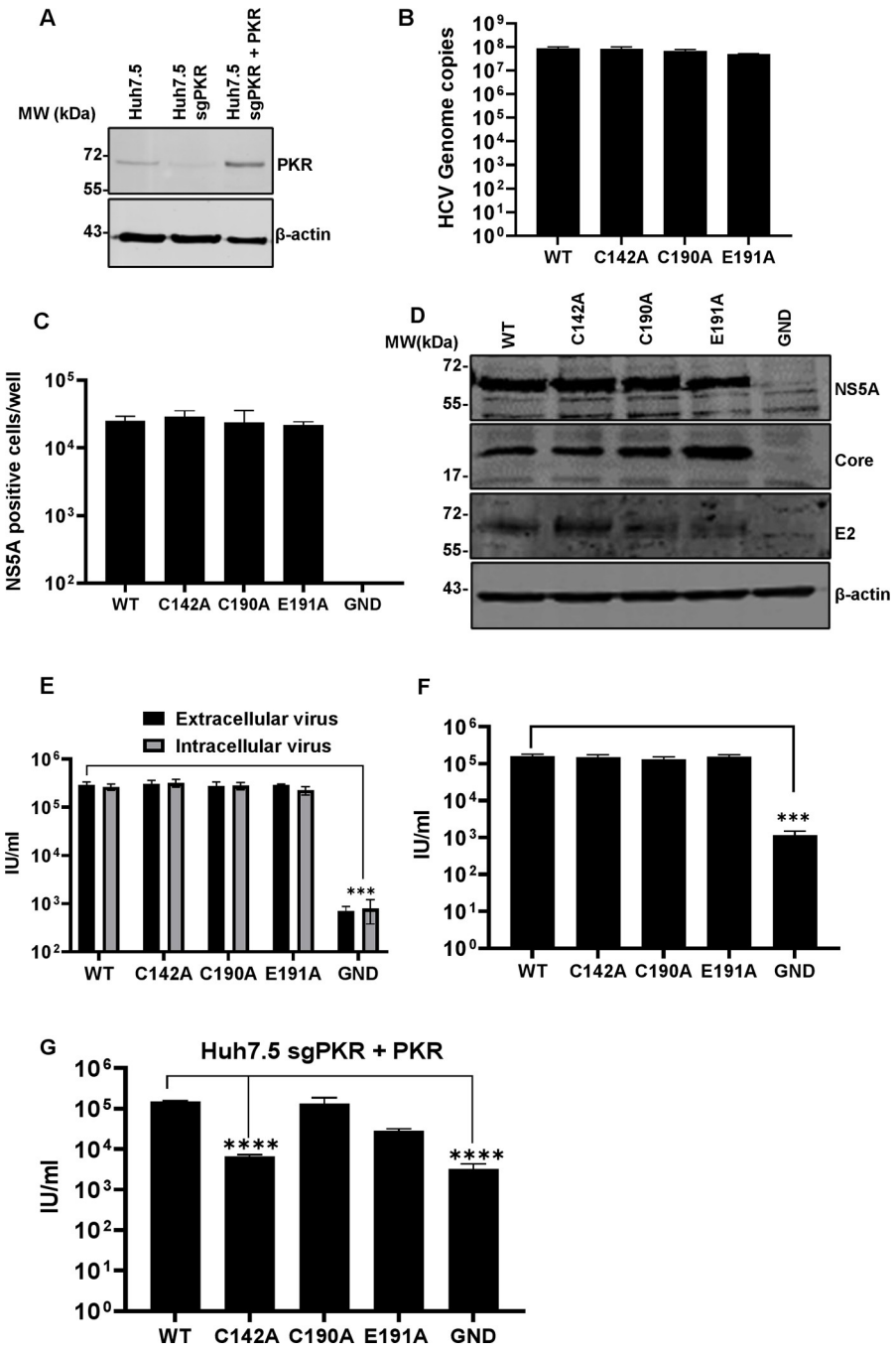

Fig 6. Virus assembly in PKR-silenced Huh7.5 cells. (A) PKR expression was detected in control Huh7.5 cells, silenced (Huh7.5 sgPKR), and cells subsequently transfected with pcDNA3.1-PKR by western blot (Huh7.5 sgPKR + PKR). (**B-F**) Huh7.5 cells were electroporated with mJFH-1 WT and DI mutant C142A, C190A and E191A RNAs, together with an NS5B GND mutant as negative control. Virus genome replication was analysed directly by quantification of genome copies in cell lysates using qRT-PCR, data shown have the GND values subtracted (**B**), and indirectly by enumerating NS5A positive cells at 72 hpe using the IncuCyte S3 (**C**). **(D)** Cell lysates were collected at 72 hpe and analysed by western blotting with the indicated antibodies. **(E)** Extra- and intracellular virus harvested at 72 hpe were titrated in Huh7.5 cells and quantified using the IncuCyte S3. (**F**) Electroporated cells were treated with the PKR inhibitor C16 (1μM) from 24 hpe, extracellular virus was harvested at 72 hpe, titrated in Huh7.5 cells and quantified using the IncuCyte S3. **(G)** Extracellular virus harvested at 72 hpe was titrated in Huh7.5 cells and quantified using the IncuCyte S3. N = 3, significant differences from WT denoted by *** ($P<0.001$) and **** ($P<0.0001$).

https://doi.org/10.1371/journal.ppat.1010812.g006

E191A compared to WT, although this was only statistically significant for C142A. Taken together, these data are consistent with a role for PKR in blocking virus assembly and point to a role of NS5A DI in antagonising this previously undefined function of PKR.

PKR silencing restores the LD phenotype of the assembly mutants

We next sought to determine whether the restoration of infectious virus production by PKR silencing was associated with concomitant changes in LD morphology, distribution and the association with NS5A and Core. We therefore repeated the confocal analysis as described for Huh7.5 cells in Figs 3–5 in the PKR-silenced cells. As shown in the representative images in Fig 7, and quantified in Fig 8, no differences between WT and the three mutants with regard to LD number and size were observed (Fig 8A), although it should be noted that overall the size of LDs in infected cells was slightly reduced (Fig 4A). Co-localisation analysis also revealed that, unlike in Huh7.5 cells, no differences were observed between WT or the three mutants in terms of their co-localisation between NS5A and LD (Fig 8B), Core and LD (Fig 8C) or NS5A and Core (Fig 8D).

Lastly, we assessed the distribution of LDs by quantifying their distance from the nucleus. As shown in the representative images in Fig 9A, and quantified in Fig 9B, the distribution of LDs in PKR silenced cells was comparable to that observed in Huh7.5 cells: in C142A and E191A infected cells LDs were significantly closer to the nucleus than WT and C190A, although still more dispersed than mock infected cells. These data are consistent with the suggestion that PKR functions to disrupt virus assembly by blocking the HCV-mediated perturbations of LD morphology. Furthermore, NS5A DI antagonises this function of PKR through the surface exposed residues C142 and E191.

Assembly defective mutants C142A and E191A exhibit altered dsRNA distribution and colocalization with PKR

We next sought to understand the differences between WT and the NS5A DI assembly-defective mutants with regard to PKR activation. PKR is activated by binding to dsRNA via two N-terminal RNA-binding domains (dsRBD) [65,66]. This leads to dimerisation of PKR, autophosphorylation and activation of the C-terminal kinase domain. Notably, dsRNA is generated as a replication intermediate and co-localises with NS5A, Core and LDs [67]. Furthermore, the HCV genome contains many structured RNA elements with extensive double-stranded regions [68]. Although genome replication is likely protected from PKR as it occurs within the membranous web [23], nascent genomes must be transported through the cytoplasm to sites of assembly and during this process may be detected by PKR. We therefore assessed the co-localisation between dsRNA, NS5A and LDs in Huh7.5 cells using a well-characterised dsRNA-specific antibody, J2 [67]. We first confirmed that this antibody was specific for dsRNA produced as a result of productive virus infection and did not detect either cellular dsRNA or the electroporated HCV RNA. Reassuringly, no signal was observed when cells electroporated with the GND replication-defective HCV RNA were stained at 4 hpe (S6D Fig). In contrast, in WT infected cells, we observed co-localisation of dsRNA with both NS5A and LDs (Fig 10). This co-localisation was also quantified in cells infected with the three mutants and surprisingly, revealed no significant differences in the co-localisation of NS5A and dsRNA (Fig 11A) or LD and dsRNA (Fig 11B). However, we did observe significant differences in the number of dsRNA foci; WT and C190A infected cells exhibited 200–300 dsRNA punctae, whereas C142A and E191A infected cells had between 100–200 punctae (Fig 11C). Taken together with the observation that the overall abundance of HCV genomes (Fig 2A), and dsRNA (Fig 11D) in all of these cells were equivalent, this suggests that for the two assembly

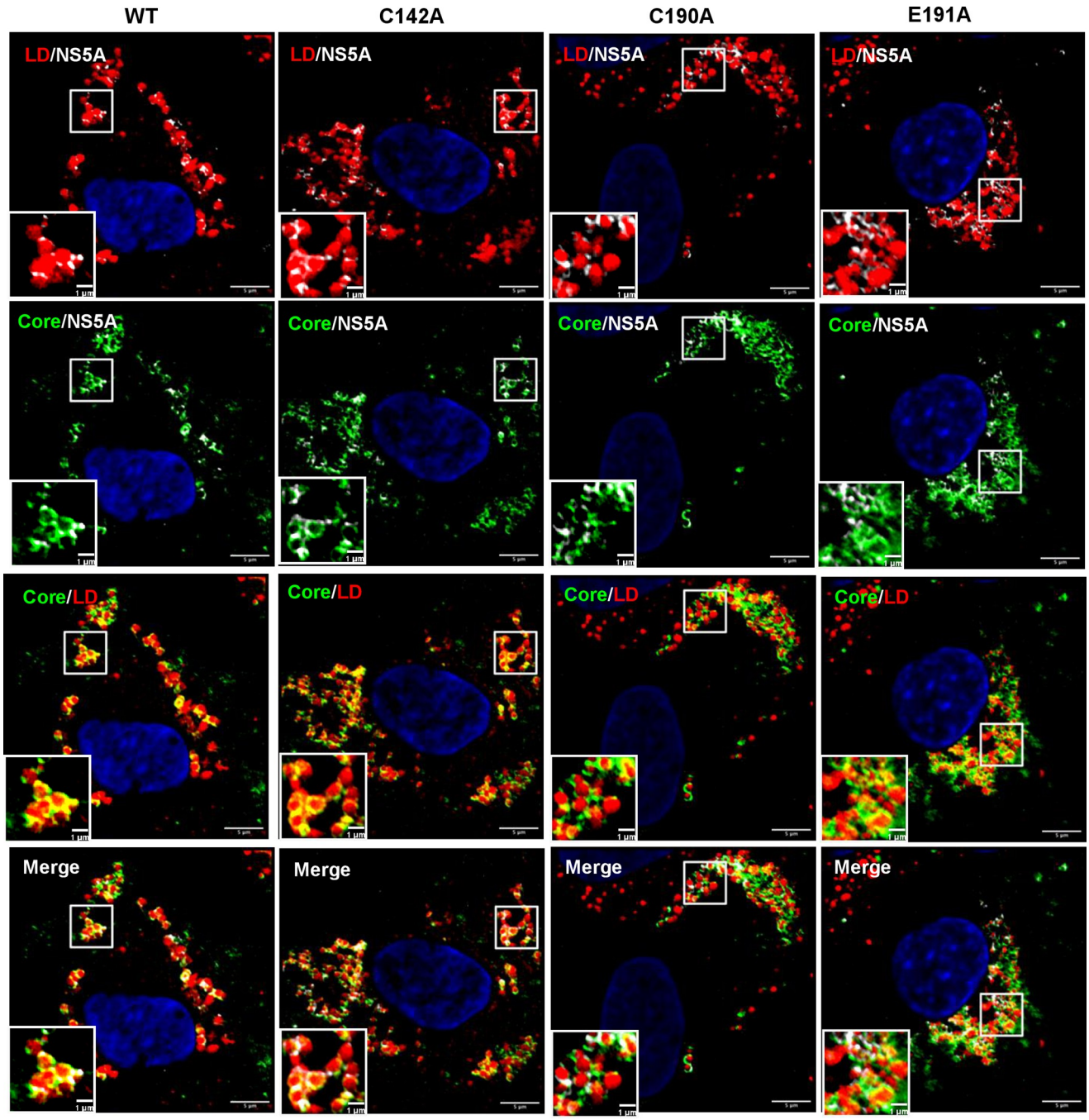

Fig 7. Co-localisation between NS5A, Core and LD in PKR-silenced Huh7.5 cells. Huh7.5 cells silenced for PKR expression were electroporated with mJFH-1 WT and DI mutant C142A, C190A and E191A RNAs and seeded on to coverslips. Cells were stained at 72 hpe with sheep anti-NS5A (white), rabbit anti-Core (green), BODIPY 558/568-C12 (red) and DAPI. Co-localisation was observed using Airyscan microscopy. Representative images are shown. Representative images of mock electroporated cells are shown in S6B Fig. Scale bars are 5 μm and 1 μm (insets).

https://doi.org/10.1371/journal.ppat.1010812.g007

defective mutants our results are consistent with a block in dsRNA trafficking to sites of virus assembly (distinct from LDs), or an accumulation of dsRNA in larger punctae.

To determine if this defect had concomitant effects on the co-localisation of NS5A and dsRNA with PKR, infected cells were analysed by immunofluorescence with antibodies to

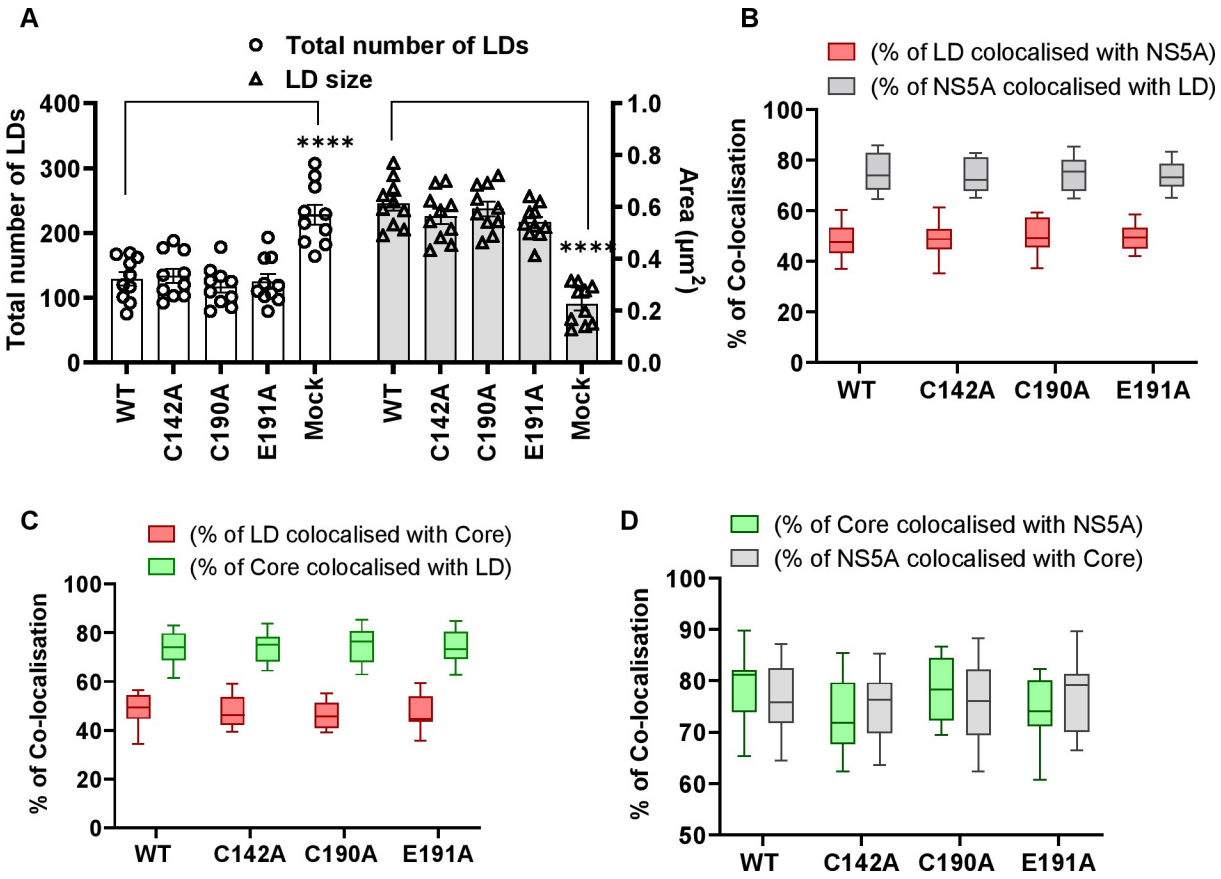

Fig 8. Quantification of LD size, abundance and co-localisation with NS5A and Core in PKR-silenced Huh7.5 cells. (A) LD numbers and size from Fig 7 were calculated using Analyze Particles module of Fiji. Mock: uninfected Huh7.5 cells. 10 cells were analysed for each sample. **(B)** Quantification of percentage of LDs colocalizing with NS5A (red), and NS5A colocalized with LD (grey). **(C)** Quantification of the percentage of LD colocalized with Core (red), and Core colocalized with LD (green). **(D)** Quantification of the percentage of Core colocalized with NS5A (green), and NS5A colocalized with Core (grey). Co-localisation was analyzed in 10 cells for each construct using Fiji. Significant differences from WT denoted by **** ($P<0.0001$).

https://doi.org/10.1371/journal.ppat.1010812.g008

NS5A, dsRNA and PKR (Fig 12A). PKR exhibited a diffuse staining pattern throughout the cytoplasm, although this was not uniform and comprised of many indistinct punctae. The co-localisation of PKR with dsRNA and NS5A was also quantified in these cells–we observed a significant decrease in the percentage of NS5A co-localised with PKR in the two assembly defective mutants (Fig 12B), together with a significant increase in the percentage of PKR co-localised with dsRNA for these mutants (Fig 12C). These data are consistent with the failure of NS5A to block PKR binding to dsRNA elements in nascent genomes, resulting in PKR activation and stimulation of an antiviral response.

NS5A DI interacts with PKR

NS5A has been previously demonstrated to directly interact with PKR via a region in D2 including the ISDR and a short region C-terminal to the ISDR [42]. These studies were performed with NS5A from genotype 1b and showed exquisite sensitivity to the amino acid sequence of the ISDR. The homology in this region between genotype 1b and JFH-1 (genotype 2a) is low (44% identity) so it is unlikely that the ISDR in JFH-1 binds to PKR, although this has not been formally proven. We considered that the ability of NS5A DI to block PKR could

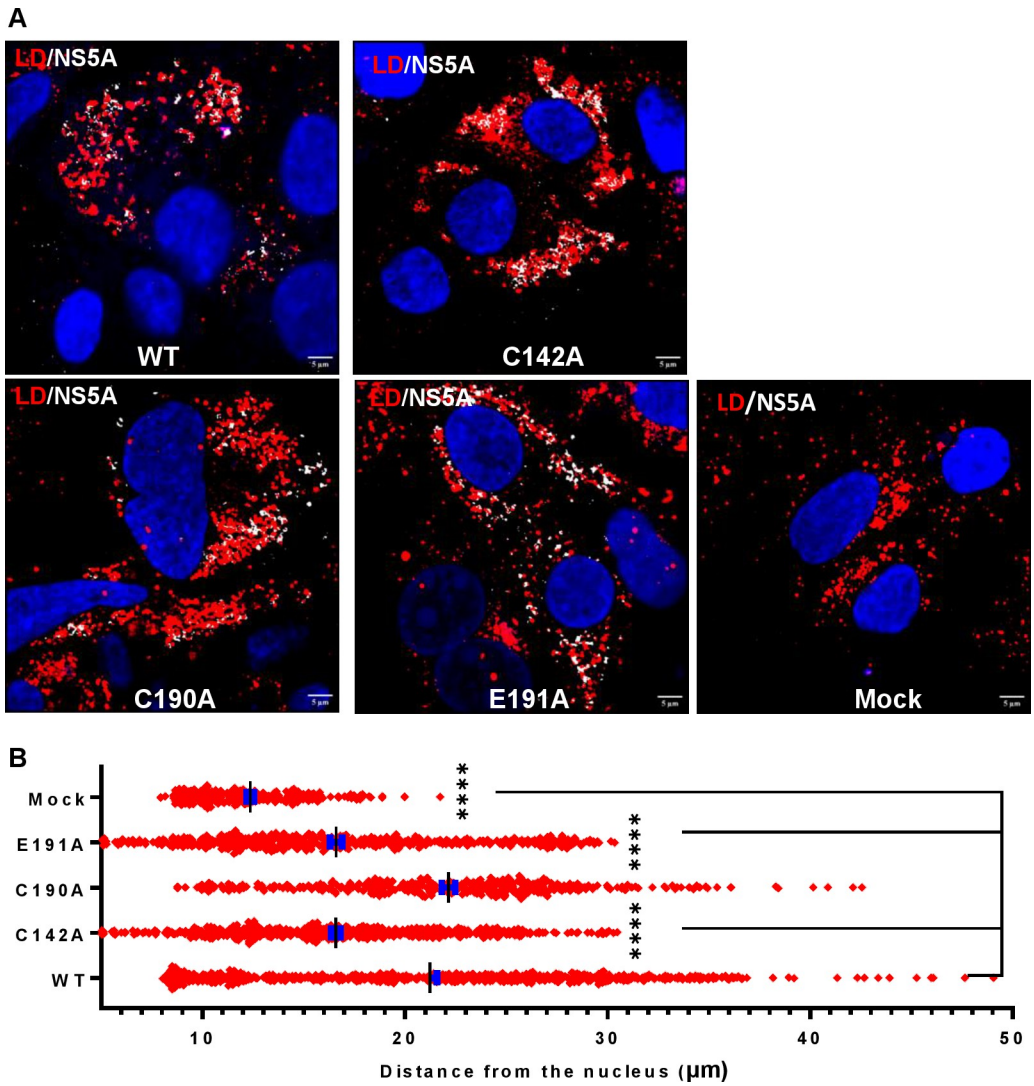

Fig 9. Analysis of LD distribution in PKR-silenced Huh7.5 cells. (A) Cells were stained at 72 hpe with sheep anti-NS5A (white), BODIPY 558/568-C12 (red) and DAPI. **(B)** Distance of LDs from the nucleus was evaluated using the Analyze Particles module of Fiji. 10 cells were analysed for each sample. Significant differences from WT denoted by **** ($P<0.0001$).

https://doi.org/10.1371/journal.ppat.1010812.g009

be explained by a direct interaction between the two proteins, dependent on C142 and E191. To test this we immunoprecipitated PKR from Huh7.5 cells electroporated with either WT or the three mutants and investigated the presence of NS5A in the immunoprecipitates by western blotting. As shown in Fig 13A, only WT and C190A NS5A co-precipitated with PKR, whereas C142A and E191A NS5A did not. The co-precipitation was weak, consistent with the immunofluorescence and co-localisation data (Fig 12) which demonstrated a much broader distribution of PKR in comparison to NS5A.

To further validate the interaction between NS5A DI and PKR, His-SUMO tagged NS5A DI (WT and mutants) were expressed in *E.coli*, purified and used as bait to precipitate PKR overexpressed in HEK293T cells. Confirming the co-immunoprecipitation data, only WT and C190A DI, but not C142A and E191A, were able to precipitate PKR from the cell lysate (Fig 13B), confirming that DI is indeed able to bind to PKR. These data are consistent with the

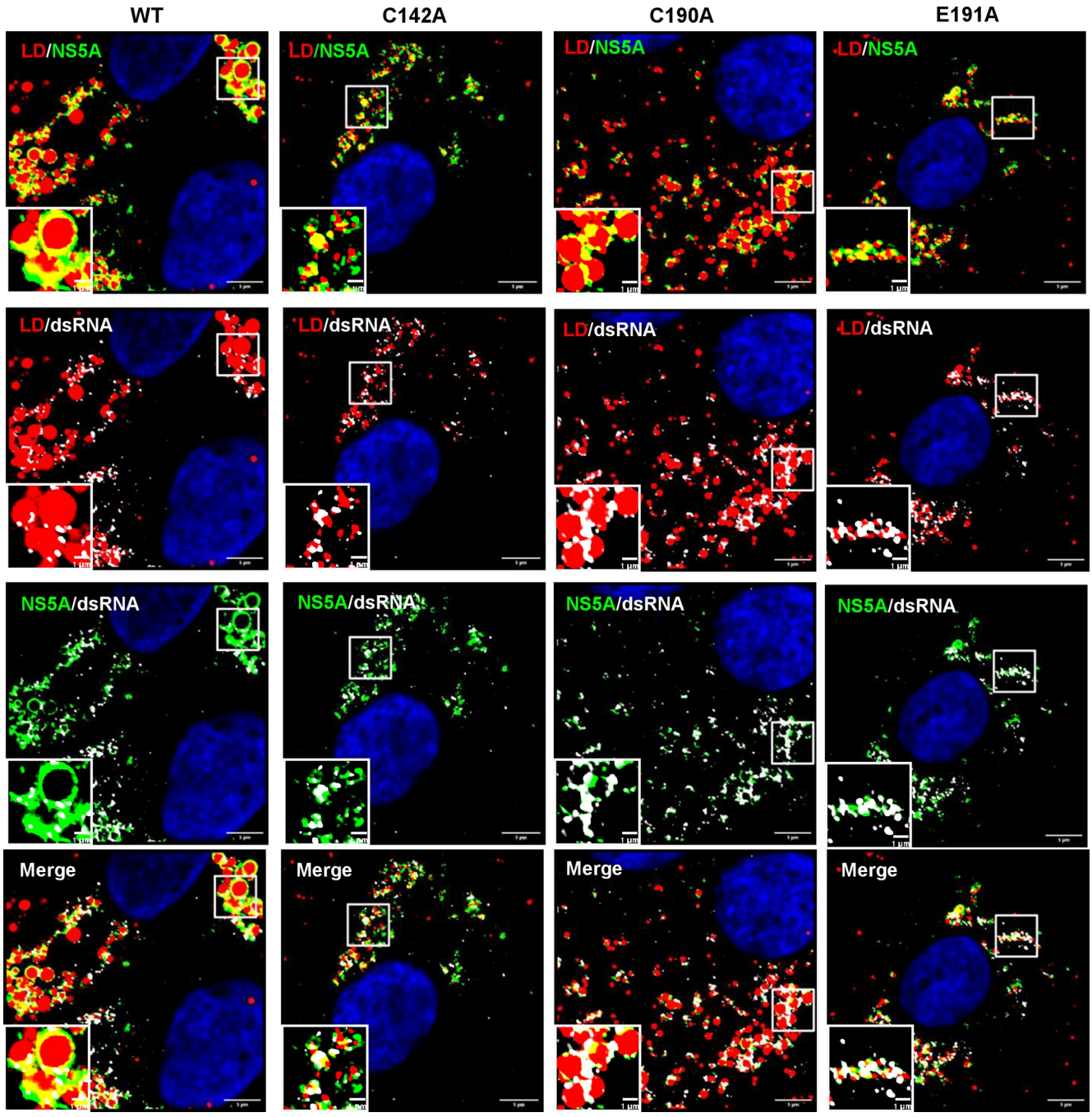

Fig 10. Co-localisation of NS5A, dsRNA and LD. Huh7.5 cells were electroporated with mJFH-1 WT and DI mutant C142A, C190A and E191A RNAs and seeded on to coverslips. At 72 hpe cells were stained with sheep anti-NS5A (green), mouse anti-dsRNA J2 (white), BODIPY 558/568-C12 (red) and DAPI. Co-localisation was observed using Airyscan microscopy. Representative images are shown. Representative images of mock electroporated cells is shown in S6C Fig. Scale bars are 5 μm and 1 μm (insets).

https://doi.org/10.1371/journal.ppat.1010812.g010

hypothesis that NS5A DI binds directly to PKR to prevent it activating downstream pathways that would lead to an antiviral response against virus assembly. We therefore turned our attention to identifying the downstream PKR effector(s) responsible.

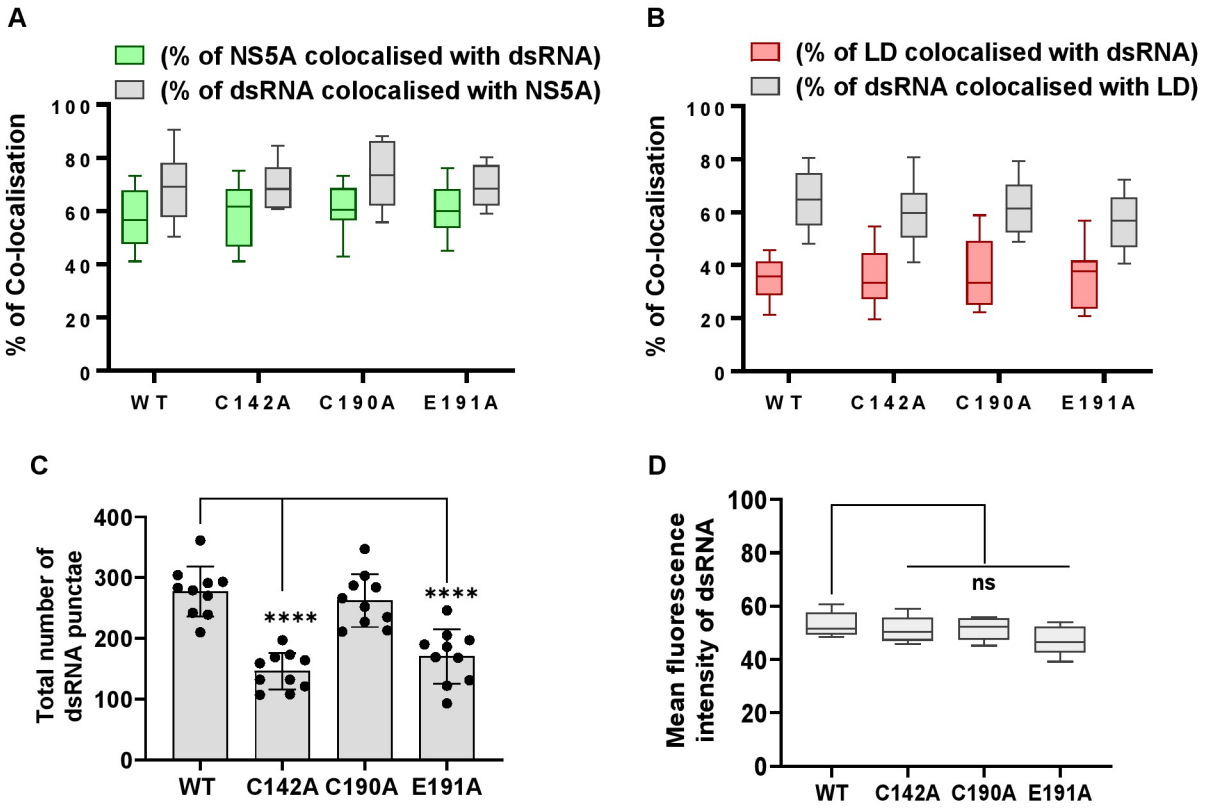

Fig 11. Quantification of dsRNA punctae and co-localisation with NS5A and LD. **(A)** Quantification of the percentage of NS5A colocalized with dsRNA (green), and dsRNA colocalized with NS5A (grey). **(B)** Quantification of the percentage of LD colocalized with dsRNA (red), and dsRNA colocalized with LD (grey). Co-localisation was analyzed in 10 cells from Fig 10 using Fiji. **(C)** Numbers of dsRNA punctae of each sample were calculated using the Analyze Particles module of Fiji. 10 cells were analysed for each sample. Significant differences from WT denoted by ns ($P>0.05$), **** ($P<0.0001$). **(D)** Total fluorescence of dsRNA staining was quantified by Fiji and presented as arbitrary units.

https://doi.org/10.1371/journal.ppat.1010812.g011

A role for the PKR effector IRF1 in blocking HCV assembly

A well characterised downstream effector of PKR is the phosphorylation of eIF2α at Ser51 to block protein synthesis. PKR also activates NFκB independently of its catalytic activity [50,51], as well as interferon regulatory factor 1 (IRF1). Although the mechanism by which PKR activates IRF1 is uncharacterised, unlike NFκB activation it is dependent on PKR catalytic activity [69].

Western blotting of infected cell lysates with antibodies to either Ser51-phosphorylated eIF2α or total eIF2α revealed no differences between WT and the three mutants (S4 Fig). As a positive control, cells were treated with tunicamycin which acts to promote eIF2α phosphorylation by inducing ER stress. We therefore concluded that eIF2α phosphorylation by PKR is not implicated in the downstream effects on HCV assembly. Activation of NFκB results in translocation of the p65 subunit from the cytoplasm to the nucleus. To test whether this downstream effector was responsible for the PKR effect on virus assembly we analysed infected cells by immunofluorescence with an antibody specific to p65 (S5 Fig). As expected, treatment with the NFκB activator TNFα resulted in efficient nuclear translocation of p65, however as shown in the representative images in S5 Fig no such translocation was observed for either mock-infected or HCV-infected cells (WT or mutants). We thus conclude that activation of NFκB by PKR is not required for its effects on virus assembly, consistent with a requirement of PKR catalytic activity for the virus assembly block (Fig 6F).

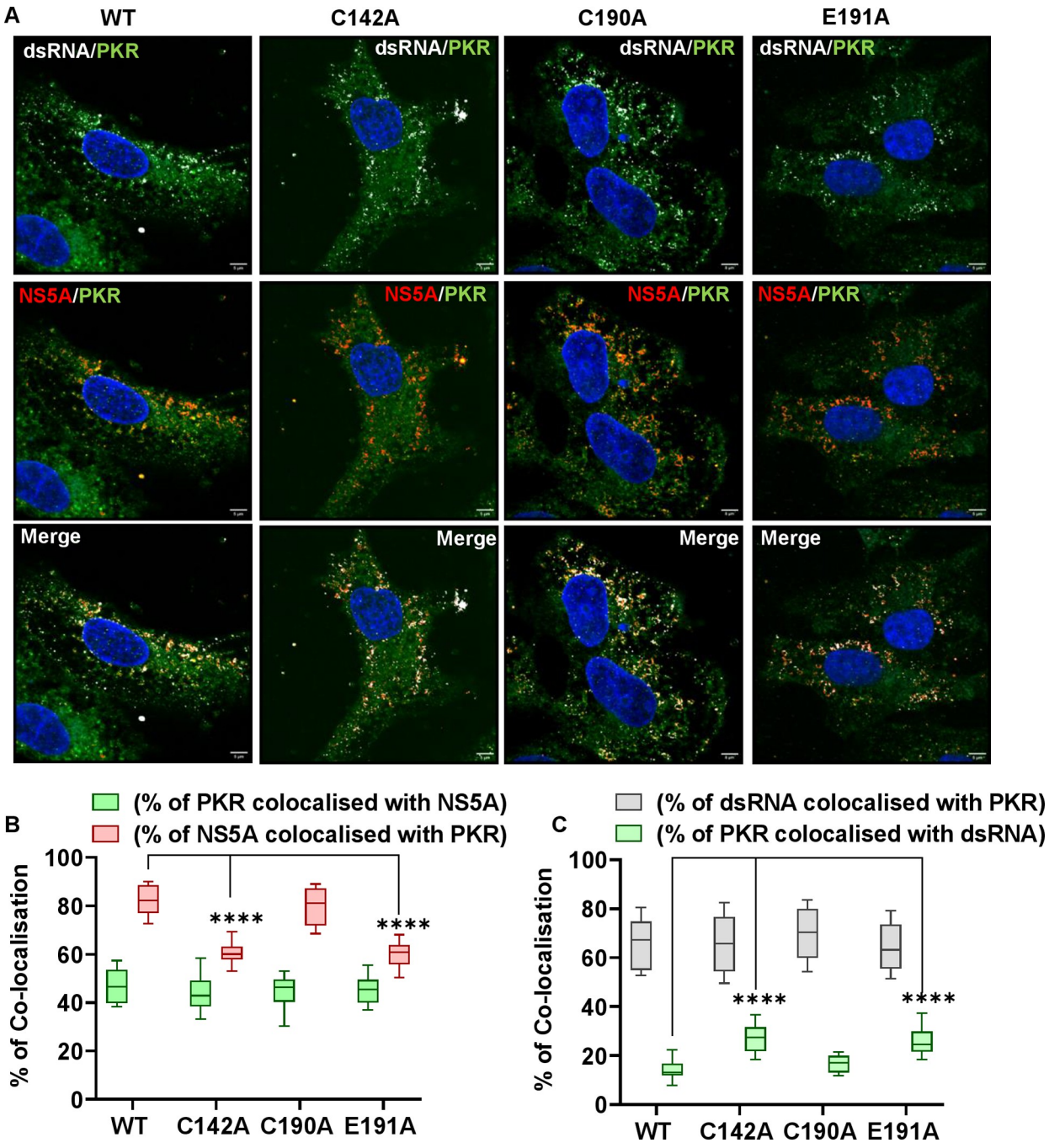

Fig 12. Co-localisation of NS5A, dsRNA and PKR. (A) Huh7.5 cells were electroporated with mJFH-1 WT and DI mutant C142A, C190A and E191A RNAs and seeded on to coverslips. At 72 hpe cells were stained with sheep anti-NS5A (red), mouse anti-dsRNA J2 (white), rabbit anti-PKR (green) and DAPI. Co-localisation was observed using Airyscan microscopy. Representative images are shown. Scale bars are 5 μm. **(B)** Quantification of the percentage of PKR colocalized with NS5A (green), and NS5A colocalized with PKR (red). **(C)** Quantification of the percentage of dsRNA colocalized with PKR (grey), and PKR colocalized with dsRNA (green). Co-localisation was analyzed in 10 cells using Fiji. Significant differences from WT denoted by **** ($P<0.0001$).

https://doi.org/10.1371/journal.ppat.1010812.g012

We finally focused on IRF1 which drives expression of antiviral interferon-stimulated genes (ISGs) [70]. IRF1 has been previously demonstrated to negatively regulate HCV genome replication [71], and the silencing of either IRF1 itself, or its effector targets immunoproteasome

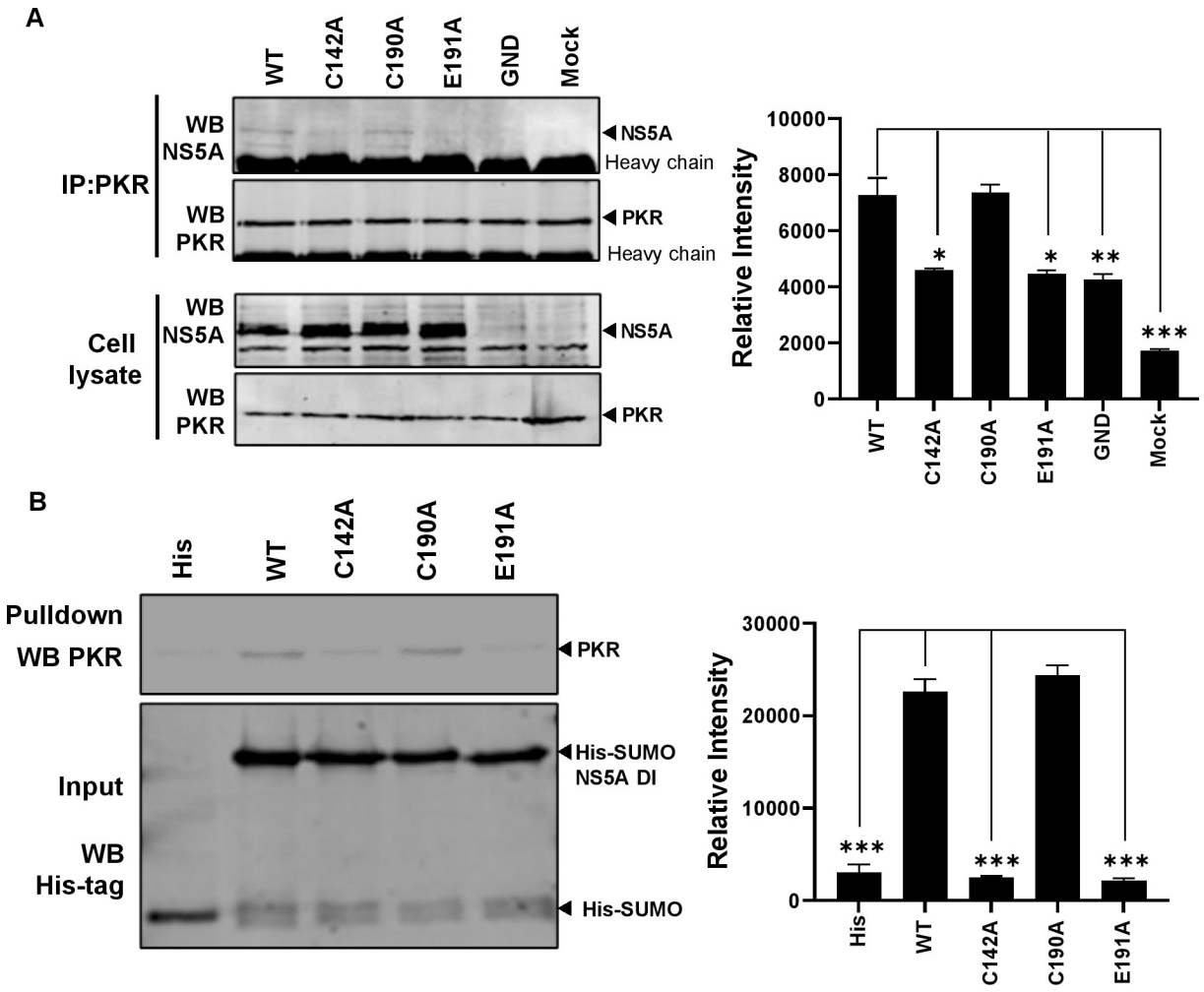

Fig 13. Protein-protein interaction analysis of NS5A and PKR. (A) Huh7.5 cells electroporated with mJFH-1 WT and DI mutants C142A, C190A and E191 were lysed and immunoprecipated with anti PKR antibody (**A**). Immunoprecipitates (top) and lysates (bottom) were analysed by western blot with the indicated antibodies. (**B**) His-SUMO tagged NS5A DI and mutants were purified and bound to Dynabead His-Tag beads as a bait to precipitate PKR protein overexpressed in HEK293T cells. Precipitates were analysed by western blotting for PKR (top), and inputs verified by western blotting for the His-tag (bottom). Representative WB are shown. Blots from 3 independent experiments were quantified by densitometry (right hand graphs). Significant differences from WT denoted by * ($P<0.05$), ** ($P<0.01$) and *** ($P<0.001$).

https://doi.org/10.1371/journal.ppat.1010812.g013

subunit beta 9 (PSMB9), apolipoprotein L1 (APOL1) and MX dynamin like GTPase 1 (MX1) enhanced HCV genome replication [72]. The effects of IRF1 on HCV assembly have not been evaluated. To test this, we silenced IRF1 in Huh7.5 cells using CRISPR/Cas9 (Fig 14A), and electroporated these cells with WT or the mutant HCV RNAs. As was observed for PKR silenced cells, genome replication (Fig 14B) and viral protein production (Fig 14C and 14D) was unaffected by the absence of IRF1. Reassuringly, when we analysed the assembly and release of the mutants, the production of infectious virus by C142A and E191A were restored to the same levels as WT and C190A in IRF1 knockout Huh7.5 cells (Fig 14E). To further confirm the direct role of IRF1, we exogenously overexpressed IRF1 in the silenced Huh7.5 cells (Fig 14A), prior to analysing release of infectious WT and mutant viruses. As shown in Fig 14F this resulted in a statistically significant reduction in titres of C142A and E191A compared to WT. Lastly, we analysed the expression of an IRF1-responsive gene previously shown to inhibit HCV genome replication, PSMB9. As shown in S7 Fig, this gene was expressed to higher levels in cells infected with C142A

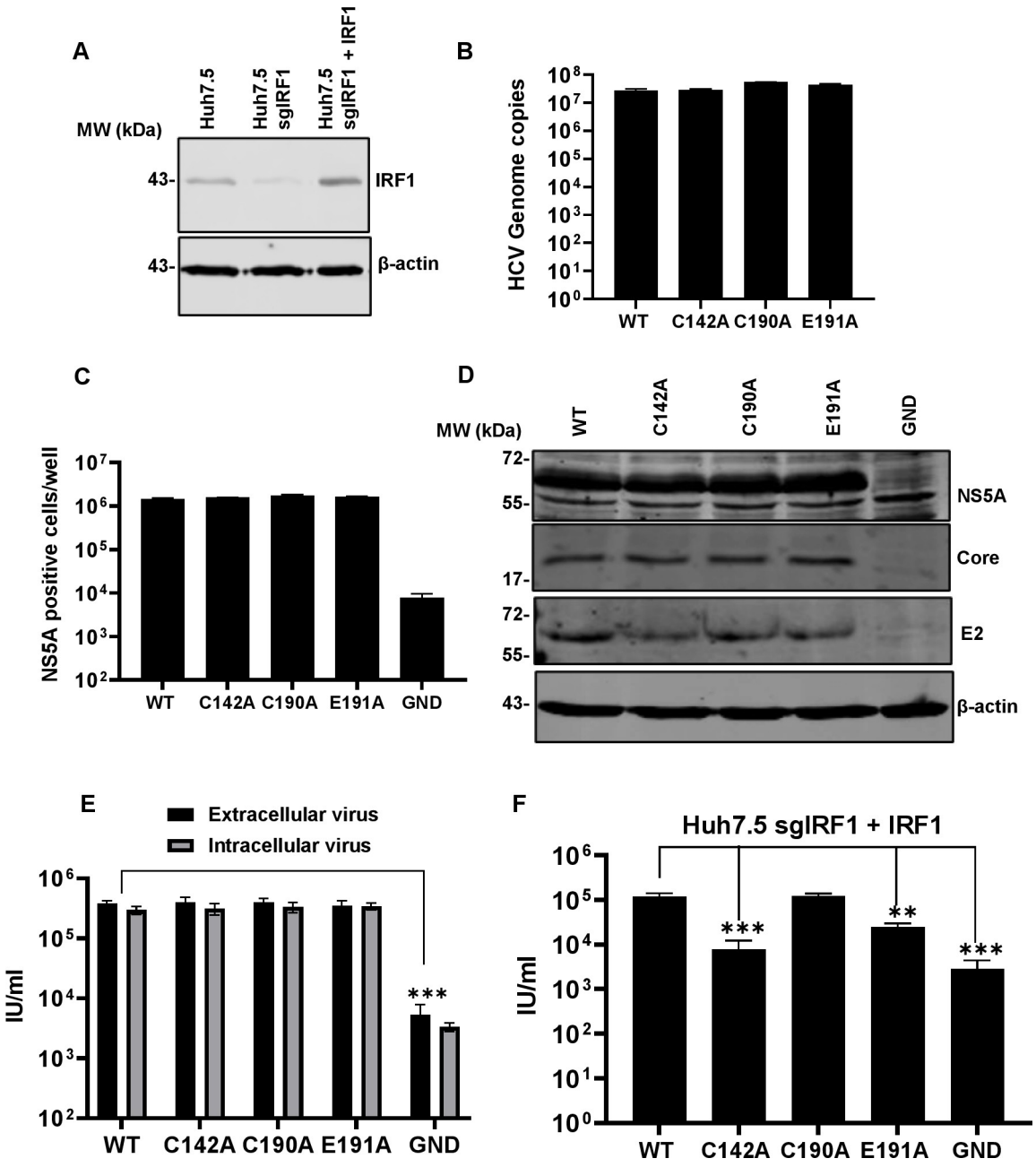

Fig 14. Virus assembly in IRF1-silenced Huh7.5 cells. (A) IRF1 expression was detected in control Huh7.5 cells, silenced (Huh7.5 sgIRF1), and cells subsequently transfected with an IRF1 expression vector (Huh7.5 sgIRF1 + IRF1) by western blot. **(B-G)** Huh7.5 cells were electroporated with mJFH-1 WT and DI mutant C142A, C190A and E191A RNAs, together with an NS5B GND mutant as negative control. Virus genome replication was analysed detected directly by quantification of genome copies in cell lysates using qRT-PCR (**B**), and indirectly by enumerating NS5A positive cells at 72 hpe using the IncuCyte S3 (**C**). **(D)** Cell lysates were collected at 72 hpe and then analysed by western blot with the indicated antibodies. **(E)**. Extra- and intracellular virus harvested at 72 hpe were titrated onto Huh7.5 cells and quantified using the IncuCyte S3. **(F)** Extracellular virus harvested at 72 hpe was titrated in Huh7.5 cells and quantified using the IncuCyte S3. N = 3, significant differences from WT denoted by ** ($P<0.01$) and *** ($P<0.001$).

https://doi.org/10.1371/journal.ppat.1010812.g014

and E191A, compared to WT and C190A, consistent with the inability of the assembly defective mutants to block PKR/IRF1 signalling. These data confirmed that the ability of PKR to inhibit the assembly of HCV is mediated by its activation of the downstream effector IRF1.

Discussion

This study builds on our previously published work [15] and provides further evidence that DI of NS5A plays a key role in HCV assembly. However, our analysis revealed that only a limited number of residues are involved in this role as only two further residues (C142 and E191) share the previously identified role in virus assembly exhibited by V67 and P145. The majority of highly conserved residues present on the surface of the NS5A DI monomer in proximity to P145 are either dispensable for virus assembly, or critical for genome replication (S1 and S2 Figs). However, it is important to note that P145A exhibited a genome replication defect in Huh7 cells which was restored in Huh7.5 cells [15]. Thus the phenotype of P145A is subtly different from C142A and E191A which exhibited no replication defect in either Huh7 or Huh7.5 cells, suggesting that the latter mutants do not precisely phenocopy P145A and cannot be directly compared. The different functions of closely located residues on the surface of NS5A is consistent with the protein mediating a switch from virus replication to assembly, perhaps by interacting with a different subset of cellular and/or viral factors. The nature of the switch remains obscure although phosphorylation of the serine cluster in the low complexity sequence linking DI and DII has been proposed. As C142 and E191 are close to the C-terminus of DI it is conceivable that they are regulated by phosphorylation. It has been hypothesised that the two dimeric forms–open (1ZH1) and closed (3FQM) represent the two conformations of NS5A with different functions. In this regard it is interesting to speculate that in the closed dimer C142 is partially occluded within the dimer interface (Fig 1C) and it is more likely for the open form to function in virus assembly.

A role for DI in virus assembly is consistent with the observation that treatment of infected cells with an NS5A DAA (ledipasvir) inhibited virus assembly within 2 h. In contrast, inhibition of genome replication was not observed until >12 h, most likely due to the inability of NS5A DAAs to inhibit pre-existing replication complexes [16]. Given that NS5A DAAs target DI, the implication of this data are that DI plays a role in assembly, as well as genome replication.

Our data show that for WT and C190A that efficiently assemble into infectious virus particles, the number of LDs per-cell is lower in comparison to mock infected cells (Fig 4). This was concomitant with an increase in the size of LDs, suggesting that virus infection coalesces LDs into larger entities that support the process of virus assembly. LDs were also distributed throughout the cytoplasm compared to the restricted perinuclear distribution observed in mock infected cells (Fig 5). These changes were not apparent for assembly defective mutants for which, the colocalisation of NS5A and Core with LDs, and the NS5A:Core colocalisation, were all reduced. Together, these data are consistent with the hypothesis that NS5A DI regulates the recruitment of both NS5A and Core to LDs, and modulates LD morphology and distribution to facilitate virus assembly.

Our observation that the silencing of PKR restored the phenotype of the two assembly defective mutants provides clues to the mechanism of action of DI in regulating assembly. NS5A binds viral RNA [25,26] and the open form [14] presents a basic surface in the groove between the monomers that is a possible RNA binding motif (Fig 1B). An attractive hypothesis is therefore that NS5A is involved in transporting nascent genomic RNA from sites of replication to sites of assembly [73,74]. In this scenario, the LD is a waystation on the route and at that point NS5A could deliver the RNA to the Core protein, rather like a baton in a relay race. One potential consequence of this is that the RNA would be transiently exposed in the cytosol, permitting detection by innate cytosolic sensors such as PKR. PKR is activated by binding to short (30 bp) dsRNA elements but can be activated by imperfect dsRNA or single stranded RNA [75]. In this regard, the HCV 5' IRES has been shown to be both a potent activator [76]

and inhibitor [77] of PKR. We postulate that DI interferes with the binding of PKR to nascent genomes, possibly by direct binding to PKR (Fig 13), preventing PKR activation and the induction of downstream antiviral pathways. However, both the co-localisation (Fig 12), and co-immunoprecipation data (Fig 13), show that the NS5A-PKR interaction is weak and/or limited by sub-cellular localisation. The data are thus consistent with NS5A interfering with a limited subset of PKR molecules, perhaps those associated with HCV derived dsRNA? PKR silencing also restored the LD phenotype (Figs 7 and 8), suggesting that activated PKR functions at the level of LD morphology to block virus assembly.

Our data suggest that neither eIF2α phosphorylation, nor activation of NFκB, are involved in the block to virus assembly (S4 and S5 Figs), although these analyses were performed at 72 hpe and we cannot rule out transient effects at earlier times. PKR also activates IRF1, the silencing of which also restores the function of the virus assembly mutants. The implication of this observation is that one or more proteins whose expression is IRF1-dependent function to block virus assembly. In this regard a recent study [72] identified a number of IRF1 regulated genes (PSMB9, ApoL1 and MX1), which when silenced enhanced HCV replication approximately 3-fold. Overexpression of PSMB9 (a component of the proteosome) led to a 10-fold reduction in HCV virus production, but a specific effect on virus assembly for ApoL1 and MX1 was not investigated. Consistent with a potential role for PSMB9, we also showed that it was expressed to higher levels in cells infected with C142A and E191A, compared to WT and C190A (S7 Fig), further supporting the hypothesis that IRF1 is driving expression of antiviral genes that could function to block virus assembly. Whilst PSMB9 may play a role, it is unlikely that it explains the 1000-fold reduction in virus production exhibited by C142A, which is completely restored by either PKR or IRF1 silencing. Of note ApoL1 (apolipoprotein L1) is an LD associated protein and, whilst other apolipoproteins have been implicated in HCV assembly (eg ApoE), the role of ApoL1 has not been investigated [78]. The recruitment of ApoL1 to LDs is regulated by DGAT-1 [79], which is required for HCV assembly and recruits both NS5A and Core to LDs [36,80]. ApoL1 may therefore be an antiviral effector induced by PKR that acts on LD morphology to block virus assembly.

In conclusion, we here provide further support for a role of NS5A DI in controlling the assembly of infectious HCV particles. Analysis of assembly-defective DI mutants revealed a hitherto unknown antiviral pathway controlled by PKR and involving the downstream effector IRF1 which results in a block to virus assembly. Current work in our laboratory is focussed on dissecting the molecular mechanisms of this block to virus assembly and identifying the key players mediating these effects.

Materials and methods

Cell lines

Huh7 (human hepatocellular carcinoma) [81] and Huh7.5 cells (a derivative of Huh7 from which a stable subgenomic replicon was 'cured' by IFN treatment and which exhibit a defect in RIG-I) [82] were used for electroporation. HEK-293T cells were used for transfections. Cells were cultured in Dulbecco's Modified Eagles Medium (DMEM; Sigma) supplemented with 10% fetal bovine serum (FBS), 100 IU penicillin/ml, 100 μg/ml streptomycin and 1% non-essential amino acids (Lonza) in a humidified incubator at 37˚C, 5% CO_2.

Plasmid and virus constructs

Sub-genomic replicons with a luciferase reporter (mSGR-luc-JFH-1) and infectious virus (mJFH-1) were described previously [56]. JFH-1 is an infectious clone of HCV genotype 2a originally derived from a patient with fulminant hepatitis. In both constructs unique BamHI/

AfeI restriction sites flank the NS5A coding sequence. NS5A mutations were constructed using Q5 Site-Directed Mutagenesis Kit (New England BioLabs; E0554S) and cloned into either mSGR-luc-JFH-1 or mJFH-1 via the BamHI/AfeI restriction sites. NS5A domain I (amino acids 35 to 215) with mutations was PCR amplified and then cloned into pET-28a-Sumo vector using BamHI/XhoI restriction sites to construct pET-28a-Sumo-NS5A DI and mutants. Lentivirus constructs for silencing of PKR and IRF1 were obtained from Prof. Greg Towers (UCL) [63]. PKR was amplified from Huh7 RNA and cloned into pcDNA3.1 vector using BamHI/XhoI restriction sites to construct pcDNA3.1-PKR. An IRF1 expression vector was obtained from Prof. Sam Wilson (Centre for Virus Research, Glasgow) [83]. Primer sequences are presented in S1 Table.

Antibodies

Rabbit anti-Core (polyclonal serum R4210) was obtained from John McLauchlan (Center for Virus Research, Glasgow), mouse-anti E2 (AP33) was obtained from Arvind Patel (Center for Virus Research, Glasgow). The following antibodies were also used: sheep-anti NS5A (in house polyclonal antiserum) [84], mouse-anti β-Actin (Sigma Aldrich; A1978), rabbit anti-PKR (Abcam; ab32052), mouse anti-dsRNA J2 (Scicons; 10010200), mouse-anti His (BIO-RAD; MCA1396GA), mouse-anti p65 (F-6) (Santa Cruz; sc-8008), rabbit anti-eIF2α (Cell Signaling; 9722S), rabbit anti-phospho eIF2α (Cell Signaling; 9721S) and rabbit anti-IRF1 (Cell Signaling; 8478S). Secondary IRDye 680 and 800 labelled antibodies were obtained from LI-COR, AlexaFluor-conjugated 488, 594 and 647 antibodies and BODIPY (558/568)-C12 dye were obtained from ThermoFisher Scientific.

Electroporation and luciferase assay

Huh7/Huh7.5 cells were washed in ice-cold PBS. Cells ($5x10^6$) were resuspended in ice-cold PBS and electroporated with 2 μg of RNA at 950 μF, 270 V. Cells were resuspended in complete media and then seeded separately into 96-well plates at $3x10^4$ cells/well, or 6-well plates at $3x10^5$ cells/well. At 4, 24, 48 and 72 h post-electroporation (hpe), cells were harvested into 30 μl or 200 μl passive lysis buffer (PLB; Promega), incubated for 15 min at room temperature and stored at -80˚C until used. Luciferase activity was assessed (Promega) on a FluoStar Optima luminometer. Data were recorded as relative light units (RLU).

IncuCyte S3 analysis

Following immunofluorescence staining for NS5A, plates were detected using an IncuCyte S3 (Essen BioScience). Viral titres were obtained by analysing the total number of virus positive cells per-well for each dilution. As this method measures the absolute number of infected cells, rather than the number of foci of infected cells, the titres are represented as infectious units per mL (IU/mL).

qRT-PCR

Total cellular RNA was harvested by lysis in TRIzol (Invitrogen) and extracted using chloroform. cDNA were synthesised from 1 μg RNA by reverse transcription using LunaScript RT SuperMix Kit (NEB; E3010). qRT-PCR was performed using Luna Universal qPCR Master Mix (NEB; M3003) with SYBR Green. Amplification was performed using the following primers: JFH-1 Forward: 5'-TCTGCGGAACCGGTGAGTA-3' JFH-1 Reverse: 5'-TCAGGCAGT ACCACAAGGC-3'.

Western blotting

Cells were washed twice in ice-cold PBS and cell lysates were harvested in 1 x GLB (1% Triton X-100, 120 mM KCl, 30 mM NaCl, 5 mM $MgCl_2$, 10% glycerol (v/v), and 10 mM piperazine-N,N'-bis (2-ethanesulfonic acid) (PIPES)-NaOH, pH 7.2) with protease and phosphatase inhibitors (Roche; 5892791001). A total of 10 or 20 μg of each sample were denatured at 95˚C for 5 min and separated by SDS-PAGE. Proteins were transferred to polyvinylidene fluoride (PVDF) membrane and blocked with 50% (v/v) Odyssey blocking buffer (LI-COR) diluted in 1X Tris-buffered saline with Tween-20 (TBS-T) (50 mM Tris-HCl pH 7.4, 150 mM NaCl, 0.1% Tween-20). Membranes were probed with primary antibodies (1:1000 dilution) at 4˚C overnight and stained with IRDye labelled anti-mouse (700 nm) and anti-rabbit (800 nm) secondary antibodies for 1 h at room temperature (RT). Membranes were imaged on a LI-COR Odyssey Sa Imager.

Virus titration

Huh7.5 cells were seeded into 96-well plates (3000 cells/well) and incubated at 37˚C overnight. The following day, freeze-thawed intracellular virus was centrifuged at 16000 rpm for 5 min and the pellets were removed. Intracellular and extracellular virus samples were serially diluted two-fold and added to Huh7.5 cells. At 48 h cells were fixed in 4% (w/v) paraformaldehyde (PFA) for 30 min and washed twice with PBS. Cells were permeabilised with 0.25% Triton X-100 (Sigma-Aldrich) in PBS for 8 min and blocked with 3% BSA diluted in PBS. Cells were probed with primary antibodies (sheep anti-NS5A 1:2000) in PBS/3% BSA at 37˚C for 1h. Cells were washed 5 times in PBS and incubated with Alexa Fluor-594 donkey anti-sheep (1:750) in PBS/3% BSA at RT for 1h. Plates were analysed using IncuCyte S3 software.

Immunofluorescence analysis

Cells were seeded onto 16 mm glass coverslips in 12 well plates, fixed, permeabilised and blocked as described above. Cells were probed with sheep anti-NS5A (1:2000), rabbit anti-Core (1:500) or mouse anti-dsRNA J2 (1:200) in PBS/3% BSA at RT for 2 h. After washing three times, cells were incubated with Alexa Fluor-488 or -647 conjugated secondary antibodies (1:500 in PBS/3% BSA) at RT in the dark for 1 h. Lipid droplets were stained with BODIPY (558/568)-C12 dye (1:1000). Cells were mounted on to glass slides with Prolong Gold antifade reagent (Invitrogen) containing 4',6'-diamidino-2-phenylindole dihydrochloride (DAPI) and sealed with nail varnish. Confocal images were acquired using a Zeiss LSM880 upright microscope with Airyscan. Post-acquisition analysis of images was performed using Fiji ImageJ (v1.49) software [85].

Quantification of LD size and distribution

LD and DAPI channels were visualised using Fiji software and merged. LD size and distribution were analysed using the Analyse Particles module of Fiji. Data were analysed using GraphPad Prism and compared using two-tailed Student's t tests.

Co-localisation analysis

Overlap coefficients were analysed by Just-Another Co-localisation Plugin (JACop) in Fiji software from 10 cells derived from three independent experiments. Data were exported to GraphPad Prism and analysed using two-tailed Student's t tests.

Lentivirus production and construction of stable knockout cell lines

HEK293T cells in 10 cm dishes were transfected with 1 μg packaging plasmid p8.91, 1 μg envelope plasmid pMDG encoding VSV-G protein and 1.5 μg transfer plasmid lenti-CRISPRv2 encoding sgRNA to either PKR or IRF1 as described [63]. Lentivirus supernatants were collected at 48 h and filtered through a 0.45 μm syringe. Huh7.5 cells were seeded into 6 well plates at density of 2.5 x 10^5 cells/well and transduced with 1 ml/well lentivirus and 8 μg/ml polybrene for 24 h. Transduced cells were selected using 2.5 μg/ml puromycin at 72 h post transduction. Loss of target protein expression was confirmed by western blotting.

Co-immunoprecipitation (Co-IP) assay

Cells were seeded into 6 well plates and lysed at 72 hpe using IP buffer (25 mM Tris-HCl pH 7.4, 150 mM NaCl, 1% NP-40, 1 mM EDTA; 5% glycerol) containing protease inhibitors for 1 h on ice. Lysates were centrifuged (13,000 × g for 5 min at 4˚C) and supernatants are precleared with 10 μl protein G beads (Invitrogen; 1004D) at 4˚C for 1 h. Cell lysates were then incubated with anti-PKR antibody at 4˚C overnight prior to addition of 20 μl protein G beads for 2 h at 4˚C. After extensive washing immunoprecipitated proteins were heat denatured at 95˚C for 5 min, separated by SDS-PAGE and analysed by western blot.

His-SUMO tagged NS5A expression, purification and pulldown assay

Plasmids were freshly transformed into *Escherichia coli* BL21 (DE3) pLysS and grown at 37˚C until OD_{600} values reached 0.6–0.8. Protein expression was induced by 100 μM isopropyl β-D-1-thiogalactopyranoside (IPTG) at 18˚C for at least 6 h. Cells were recovered by centrifugation at 8000 x g for 15 min and resuspended in 50 ml binding buffer (100 mM Tris pH 8.2, 200 mM NaCl, 20 mM imidazole) supplemented with 40 μl DNase, 40 μl RNaseA, 2 mg/ml Lysozyme and protease inhibitors (Roche) per 1 L of pelleted culture. After incubation on ice for 30 min, samples were sonicated at an amplitude of 10 microns for 12 pulses of 20 sec separated by 20 sec on ice. After centrifugation at 4000 x g for 1 h at 4˚C twice, supernatants were filtered through a 0.45 μm syringe filter. Samples were transferred to a 1 ml HisTrap FF column (Cytiva; 17531901) equilibrated with binding buffer and the column was washed 3 times using 5 column volumes of binding buffer. The samples were eluted with binding buffer containing 250 mM imidazole and dialyzed against 20 mM Tris-HCl, pH 8.2, 150 mM NaCl and 10% (v/v) glycerol.

His-SUMO tagged NS5A DI (5 μg) was diluted using 1x binding & wash buffer (BWB: 50 mM sodium phosphate pH 8.0, 300 mM NaCl, 0.02% Tween-20) and added to 20 μl Dynabead His-Tag beads (ThermoFisher Scientific; 10103D). After incubation on a roller at 4˚C for 1 h, the beads were washed 5 times with BWB at 4˚C. Lysates from pcDNA3.1-PKR transfected HEK293 cells were diluted with 1x pulldown buffer (3.25 mM Sodium-phosphate pH 7.4, 70 mM NaCl, 0.02% Tween-20) and added to the His-Tag beads at 4˚C for 2 h. Beads were washed 5 times with BWB at 4˚C, heat denatured at 95˚C for 5 min, separated by SDS-PAGE and analysed by western blot.

Statistical analysis

Statistical analysis was performed using an unpaired two-tailed Student's t tests on GraphPad Prism version 9.30. **** ($P<0.0001$), *** ($P<0.001$), ** ($P<0.01$) and * ($P<0.05$) indicate significant difference from wild type ($n>=3$). Data in histograms are displayed as the means ± S.E.

Supporting information

S1 Fig. Genome replication in Huh7 and Huh7.5 cells. *In vitro* transcribed mSGR-luc-JFH-1 RNAs containing the indicated mutations were electroporated into **(A)** Huh7 and **(B)** Huh7.5 cells. Luciferase activity was measured at 4, 24, 48 and 72 hpe and the data were normalized with respect to 4 hpe. N = 3, significant differences from WT denoted by **** ($P<0.0001$).
(PDF)

S2 Fig. Virus assembly phenotypes in Huh7.5 cells. Huh7.5 cells were electroporated with mJFH-1 WT and the DI mutant RNAs as indicated, together with an NS5B GND mutant as negative control. Extracellular virus harvested at 72 hpe was titrated in Huh7.5 cells and quantified using the IncuCyte S3. N = 3, significant difference from WT denoted by *** ($P<0.001$).
(PDF)

S3 Fig. Location of mutated residues in DI. The three surface exposed residues C142A, C190A and E191A proximal to P145 are displayed in two NS5A DI (genotype 1b) structures 1ZH1 (**A)** and 3FQM (**B).** Images on the right are zoomed into the boxed region shown in both space fill and ribbon format. Note that the disulphide bond formed by C142A and C190A was only observed in 1ZH1.
(PDF)

S4 Fig. Expression of eIF2α and phospho-eIF2α. Huh7.5 cells were electroporated with mJFH-1 WT and DI mutant C142A, C190A and E191A RNAs, together with an NS5B GND mutant as negative control. TM: tunicamycin positive control. Cells were harvested at 72 hpe and lysed with GLB. eIF2α and phospho-eIF2α was analyzed by western blotting.
(PDF)

S5 Fig. NF-κB activation in Huh7.5 cells infected with mJFH-1 or DI mutants. Huh7.5 cells were electroporated with mJFH-1 WT and DI mutants C142A, C190A and E191A RNAs. At 72 hpe, cells were fixed and stained with mouse anti-P65 (green), sheep anti-NS5A (red) and DAPI. As a positive control to activate the NF-κB pathway uninfected Huh7.5 cells were treated with TNF-α for 24h. Mock: uninfected Huh7.5 cells.
(PDF)

S6 Fig. Immunofluorescent images of uninfected Huh7.5 cells. (A) Representative image of mock infected cell from Fig 3 stained at 72 hpe with sheep anti-NS5A (white), rabbit anti-Core (green), BODIPY 558/568-C12 (red) and DAPI. Scale bar 5 μm. **(B)** Representative image of mock infected cell from Fig 7 stained at 72 hpe with sheep anti-NS5A (white), rabbit anti-Core (green), BODIPY 558/568-C12 (red) and DAPI. Scale bar 5 μm. **(C)** Representative image of mock infected cell from Fig 10 stained at 72 hpe with sheep anti-NS5A (green), mouse anti-dsRNA J2 (white), BODIPY 558/568-C12 (red) and DAPI. **(D)** Representative image of HCV NS5B GND mutant electroporated cell stained at 4 hpe with sheep anti-NS5A (green), mouse anti-dsRNA J2 (white), BODIPY 558/568-C12 (red) and DAPI. Scale bar 5 μm.
(PDF)

S7 Fig. Expression of an IRF1-responsive gene, PSMB9. Huh7.5 cells were electroporated with mJFH-1 WT and DI mutant C142A, C190A and E191A RNAs. The uninfected Huh7.5 cells (Mock) were used as a negative control. The expression of PSMB9 and GAPDH were analysed using qRT-PCR. The relative expression levels of PSMB9 in WT and mutants were compared to mock and shown as $Log_2\ 2^{-\Delta\Delta Ct}$ fold change.
(PDF)

S1 Table. oligonucleotide sequence of primers used in this study.
(PDF)

Acknowledgments

We thank Prof. Greg Towers (University College, London) for the PKR, CypA and IRF1 silencing lentivirus constructs, Prof. Sam Wilson (CVR, Glasgow) for the IRF1 expression construct, Prof John McLauchlan (CVR, Glasgow) for the anti-Core antibody and Prof Arvind Patel (CVR, Glasgow) for the AP33 anti-E2 antibody. We thank Dr Niluka Goonawardane and Dr Ruth Hughes for help in Fiji ImageJ analysis. The Zeiss LSM880 confocal microscope and Incucyte S3 were funded by Wellcome multi-user equipment grants (WT104818MA and 221538/Z/20/Z).

Author Contributions

Conceptualization: Shucheng Chen, Mark Harris.

Formal analysis: Shucheng Chen, Mark Harris.

Funding acquisition: Mark Harris.

Investigation: Shucheng Chen.

Supervision: Mark Harris.

Writing – original draft: Shucheng Chen, Mark Harris.

Writing – review & editing: Shucheng Chen, Mark Harris.

References

1. Simmonds P, Becher P, Bukh J, Gould EA, Meyers G, Monath T, et al. ICTV virus taxonomy profile: Flaviviridae. The Journal of general virology. 2017; 98(1):2. https://doi.org/10.1099/jgv.0.000672 PMID: 28218572
2. Axley P, Ahmed Z, Ravi S, Singal AK. Hepatitis C virus and hepatocellular carcinoma: a narrative review. Journal of clinical and translational hepatology. 2018; 6(1):79. https://doi.org/10.14218/JCTH.2017.00067 PMID: 29607308
3. Lingala S, Ghany MG. Natural history of hepatitis C. Gastroenterology Clinics. 2015; 44(4):717–34. https://doi.org/10.1016/j.gtc.2015.07.003 PMID: 26600216
4. Organization WH. Global hepatitis report 2017: World Health Organization. Accessed October. 2017; 23:2020.
5. Bidell MR, McLaughlin M, Faragon J, Morse C, Patel N. Desirable characteristics of hepatitis C treatment regimens: a review of what we have and what we need. Infectious diseases and therapy. 2016; 5 (3):299–312. https://doi.org/10.1007/s40121-016-0118-x PMID: 27384319
6. Adams RL, Pirakitikulr N, Pyle AM. Functional RNA structures throughout the Hepatitis C Virus genome. Current opinion in virology. 2017; 24:79–86. https://doi.org/10.1016/j.coviro.2017.04.007 PMID: 28511116
7. Penin F, Dubuisson J, Rey FA, Moradpour D, Pawlotsky JM. Structural biology of hepatitis C virus. Hepatology. 2004; 39(1):5–19. https://doi.org/10.1002/hep.20032 PMID: 14752815
8. Moradpour D, Penin F. Hepatitis C virus proteins: from structure to function. Hepatitis C virus: from molecular virology to antiviral therapy. 2013:113–42. https://doi.org/10.1007/978-3-642-27340-7_5 PMID: 23463199
9. Brass V, Bieck E, Montserret R, Wölk B, Hellings JA, Blum HE, et al. An amino-terminal amphipathic α-helix mediates membrane association of the hepatitis C virus nonstructural protein 5A. Journal of Biological Chemistry. 2002; 277(10):8130–9.
10. Penin F, Brass V, Appel N, Ramboarina S, Montserret R, Ficheux D, et al. Structure and function of the membrane anchor domain of hepatitis C virus nonstructural protein 5A. Journal of Biological Chemistry. 2004; 279(39):40835–43. https://doi.org/10.1074/jbc.M404761200 PMID: 15247283

11. Tellinghuisen TL, Marcotrigiano J, Gorbalenya AE, Rice CM. The NS5A protein of hepatitis C virus is a zinc metalloprotein. Journal of Biological Chemistry. 2004; 279(47):48576–87. https://doi.org/10.1074/jbc.M407787200 PMID: 15339921

12. Love RA, Brodsky O, Hickey MJ, Wells PA, Cronin CN. Crystal structure of a novel dimeric form of NS5A domain I protein from hepatitis C virus. Journal of virology. 2009; 83(9):4395–403. https://doi.org/10.1128/JVI.02352-08 PMID: 19244328

13. Lambert SM, Langley DR, Garnett JA, Angell R, Hedgethorne K, Meanwell NA, et al. The crystal structure of NS5A domain 1 from genotype 1a reveals new clues to the mechanism of action for dimeric HCV inhibitors. Protein Science. 2014; 23(6):723–34. https://doi.org/10.1002/pro.2456 PMID: 24639329

14. Tellinghuisen TL, Marcotrigiano J, Rice CM. Structure of the zinc-binding domain of an essential component of the hepatitis C virus replicase. Nature. 2005; 435(7040):374–9. https://doi.org/10.1038/nature03580 PMID: 15902263

15. Yin C, Goonawardane N, Stewart H, Harris M. A role for domain I of the hepatitis C virus NS5A protein in virus assembly. PLoS pathogens. 2018; 14(1):e1006834. https://doi.org/10.1371/journal.ppat.1006834 PMID: 29352312

16. McGivern DR, Masaki T, Williford S, Ingravallo P, Feng Z, Lahser F, et al. Kinetic analyses reveal potent and early blockade of hepatitis C virus assembly by NS5A inhibitors. Gastroenterology. 2014; 147(2):453–62. e7. https://doi.org/10.1053/j.gastro.2014.04.021 PMID: 24768676

17. Kapoor A, Simmonds P, Gerold G, Qaisar N, Jain K, Henriquez JA, et al. Characterization of a canine homolog of hepatitis C virus. Proceedings of the National Academy of Sciences. 2011; 108(28):11608–13. https://doi.org/10.1073/pnas.1101794108 PMID: 21610165

18. Kapoor A, Simmonds P, Scheel TK, Hjelle B, Cullen JM, Burbelo PD, et al. Identification of rodent homologs of hepatitis C virus and pegiviruses. MBio. 2013; 4(2):e00216–13. https://doi.org/10.1128/mBio.00216-13 PMID: 23572554

19. Lauck M, Sibley SD, Lara J, Purdy MA, Khudyakov Y, Hyeroba D, et al. A novel hepacivirus with an unusually long and intrinsically disordered NS5A protein in a wild Old World primate. Journal of virology. 2013; 87(16):8971–81. https://doi.org/10.1128/JVI.00888-13 PMID: 23740998

20. Smith DB, Bukh J, Kuiken C, Muerhoff AS, Rice CM, Stapleton JT, et al. Expanded classification of hepatitis C virus into 7 genotypes and 67 subtypes: updated criteria and genotype assignment web resource. Hepatology. 2014; 59(1):318–27. https://doi.org/10.1002/hep.26744 PMID: 24115039

21. Egger D, Wölk B, Gosert R, Bianchi L, Blum HE, Moradpour D, et al. Expression of hepatitis C virus proteins induces distinct membrane alterations including a candidate viral replication complex. Journal of virology. 2002; 76(12):5974–84. https://doi.org/10.1128/jvi.76.12.5974-5984.2002 PMID: 12021330

22. Miller S, Krijnse-Locker J. Modification of intracellular membrane structures for virus replication. Nature Reviews Microbiology. 2008; 6(5):363–74. https://doi.org/10.1038/nrmicro1890 PMID: 18414501

23. Paul D, Bartenschlager R. Flaviviridae replication organelles: oh, what a tangled web we weave. Annu Rev Virol. 2015; 2(1):289–310. https://doi.org/10.1146/annurev-virology-100114-055007 PMID: 26958917

24. Paul D, Madan V, Bartenschlager R. Hepatitis C virus RNA replication and assembly: living on the fat of the land. Cell host & microbe. 2014; 16(5):569–79. https://doi.org/10.1016/j.chom.2014.10.008 PMID: 25525790

25. Foster TL, Belyaeva T, Stonehouse NJ, Pearson AR, Harris M. All three domains of the hepatitis C virus nonstructural NS5A protein contribute to RNA binding. Journal of virology. 2010; 84(18):9267–77. https://doi.org/10.1128/JVI.00616-10 PMID: 20592076

26. Huang L, Hwang J, Sharma SD, Hargittai MR, Chen Y, Arnold JJ, et al. Hepatitis C virus nonstructural protein 5A (NS5A) is an RNA-binding protein. Journal of Biological Chemistry. 2005; 280(43):36417–28. https://doi.org/10.1074/jbc.M508175200 PMID: 16126720

27. Berger KL, Cooper JD, Heaton NS, Yoon R, Oakland TE, Jordan TX, et al. Roles for endocytic trafficking and phosphatidylinositol 4-kinase III alpha in hepatitis C virus replication. Proceedings of the National Academy of Sciences. 2009; 106(18):7577–82. https://doi.org/10.1073/pnas.0902693106 PMID: 19376974

28. Evans MJ, Rice CM, Goff SP. Phosphorylation of hepatitis C virus nonstructural protein 5A modulates its protein interactions and viral RNA replication. Proceedings of the National Academy of Sciences. 2004; 101(35):13038–43. https://doi.org/10.1073/pnas.0405152101 PMID: 15326295

29. Gao L, Aizaki H, He J-W, Lai MM. Interactions between viral nonstructural proteins and host protein hVAP-33 mediate the formation of hepatitis C virus RNA replication complex on lipid raft. Journal of virology. 2004; 78(7):3480–8. https://doi.org/10.1128/jvi.78.7.3480-3488.2004 PMID: 15016871

30. Hamamoto I, Nishimura Y, Okamoto T, Aizaki H, Liu M, Mori Y, et al. Human VAP-B is involved in hepatitis C virus replication through interaction with NS5A and NS5B. Journal of virology. 2005; 79(21):13473–82. https://doi.org/10.1128/JVI.79.21.13473-13482.2005 PMID: 16227268

31. Ngure M, Issur M, Shkriabai N, Liu H-W, Cosa G, Kvaratskhelia M, et al. Interactions of the disordered domain II of hepatitis C virus NS5A with cyclophilin A, NS5B, and viral RNA show extensive overlap. ACS Infectious Diseases. 2016; 2(11):839–51. https://doi.org/10.1021/acsinfecdis.6b00143 PMID: 27676132

32. Reiss S, Harak C, Romero-Brey I, Radujkovic D, Klein R, Ruggieri A, et al. The lipid kinase phosphatidylinositol-4 kinase III alpha regulates the phosphorylation status of hepatitis C virus NS5A. PLoS pathogens. 2013; 9(5):e1003359. https://doi.org/10.1371/journal.ppat.1003359 PMID: 23675303

33. Masaki T, Suzuki R, Murakami K, Aizaki H, Ishii K, Murayama A, et al. Interaction of hepatitis C virus nonstructural protein 5A with core protein is critical for the production of infectious virus particles. Journal of virology. 2008; 82(16):7964–76. https://doi.org/10.1128/JVI.00826-08 PMID: 18524832

34. Miyanari Y, Atsuzawa K, Usuda N, Watashi K, Hishiki T, Zayas M, et al. The lipid droplet is an important organelle for hepatitis C virus production. Nature cell biology. 2007; 9(9):1089–97. https://doi.org/10.1038/ncb1631 PMID: 17721513

35. Amako Y, Sarkeshik A, Hotta H, Yates J III, Siddiqui A. Role of oxysterol binding protein in hepatitis C virus infection. Journal of virology. 2009; 83(18):9237–46. https://doi.org/10.1128/JVI.00958-09 PMID: 19570870

36. Camus G, Herker E, Modi AA, Haas JT, Ramage HR, Farese RV, et al. Diacylglycerol acyltransferase-1 localizes hepatitis C virus NS5A protein to lipid droplets and enhances NS5A interaction with the viral capsid core. Journal of Biological Chemistry. 2013; 288(14):9915–23. https://doi.org/10.1074/jbc.M112.434910 PMID: 23420847

37. Guo M, Pei R, Yang Q, Cao H, Wang Y, Wu C, et al. Phosphatidylserine-specific phospholipase A1 involved in hepatitis C virus assembly through NS2 complex formation. Journal of virology. 2015; 89 (4):2367–77. https://doi.org/10.1128/JVI.02982-14 PMID: 25505071

38. Rösch K, Kwiatkowski M, Hofmann S, Schöbel A, Grüttner C, Wurlitzer M, et al. Quantitative lipid droplet proteome analysis identifies annexin A3 as a cofactor for HCV particle production. Cell reports. 2016; 16(12):3219–31. https://doi.org/10.1016/j.celrep.2016.08.052 PMID: 27653686

39. Salloum S, Wang H, Ferguson C, Parton RG, Tai AW. Rab18 binds to hepatitis C virus NS5A and promotes interaction between sites of viral replication and lipid droplets. PLoS pathogens. 2013; 9(8): e1003513. https://doi.org/10.1371/journal.ppat.1003513 PMID: 23935497

40. Vogt DA, Camus G, Herker E, Webster BR, Tsou C-L, Greene WC, et al. Lipid droplet-binding protein TIP47 regulates hepatitis C Virus RNA replication through interaction with the viral NS5A protein. PLoS pathogens. 2013; 9(4):e1003302. https://doi.org/10.1371/journal.ppat.1003302 PMID: 23593007

41. Cesaro T, Michiels T. Inhibition of PKR by Viruses. Frontiers in microbiology. 2021;12. https://doi.org/10.3389/fmicb.2021.757238 PMID: 34759908

42. Gale M Jr, Blakely CM, Kwieciszewski B, Tan S-L, Dossett M, Tang NM, et al. Control of PKR protein kinase by hepatitis C virus nonstructural 5A protein: molecular mechanisms of kinase regulation. Molecular and cellular biology. 1998; 18(9):5208–18. https://doi.org/10.1128/MCB.18.9.5208 PMID: 9710605

43. Gale MJ Jr, Korth MJ, Tang NM, Tan S-L, Hopkins DA, Dever TE, et al. Evidence that hepatitis C virus resistance to interferon is mediated through repression of the PKR protein kinase by the nonstructural 5A protein. Virology. 1997; 230(2):217–27. https://doi.org/10.1006/viro.1997.8493 PMID: 9143277

44. Wang C, Pflugheber J, Sumpter R Jr, Sodora DL, Hui D, Sen GC, et al. Alpha interferon induces distinct translational control programs to suppress hepatitis C virus RNA replication. Journal of virology. 2003; 77(7):3898–912. https://doi.org/10.1128/jvi.77.7.3898-3912.2003 PMID: 12634350

45. Arnaud N, Dabo S, Maillard P, Budkowska A, Kalliampakou KI, Mavromara P, et al. Hepatitis C virus controls interferon production through PKR activation. PloS one. 2010; 5(5):e10575. https://doi.org/10.1371/journal.pone.0010575 PMID: 20485506

46. Arnaud N, Dabo S, Akazawa D, Fukasawa M, Shinkai-Ouchi F, Hugon J, et al. Hepatitis C virus reveals a novel early control in acute immune response. PLoS pathogens. 2011; 7(10):e1002289. https://doi.org/10.1371/journal.ppat.1002289 PMID: 22022264

47. Meurs EF, Watanabe Y, Kadereit S, Barber GN, Katze MG, Chong K, et al. Constitutive expression of human double-stranded RNA-activated p68 kinase in murine cells mediates phosphorylation of eukaryotic initiation factor 2 and partial resistance to encephalomyocarditis virus growth. Journal of virology. 1992; 66(10):5805–14. https://doi.org/10.1128/JVI.66.10.5805-5814.1992 PMID: 1382142

48. Pathak V, Schindler D, Hershey J. Generation of a mutant form of protein synthesis initiation factor eIF-2 lacking the site of phosphorylation by eIF-2 kinases. Molecular and cellular biology. 1988; 8(2):993–5. https://doi.org/10.1128/mcb.8.2.993-995.1988 PMID: 3352609

49. Sudhakar A, Ramachandran A, Ghosh S, Hasnain SE, Kaufman RJ, Ramaiah KV. Phosphorylation of serine 51 in initiation factor 2α (eIF2α) promotes complex formation between eIF2α (P) and eIF2B and causes inhibition in the guanine nucleotide exchange activity of eIF2B. Biochemistry. 2000; 39 (42):12929–38.

50. Bonnet MC, Daurat C, Ottone C, Meurs EF. The N-terminus of PKR is responsible for the activation of the NF-κB signaling pathway by interacting with the IKK complex. Cellular signalling. 2006; 18 (11):1865–75.

51. Bonnet MC, Weil R, Dam E, Hovanessian AG, Meurs EF. PKR stimulates NF-κB irrespective of its kinase function by interacting with the IκB kinase complex. Molecular and cellular biology. 2000; 20 (13):4532–42.

52. Kumar A, Haque J, Lacoste J, Hiscott J, Williams B. Double-stranded RNA-dependent protein kinase activates transcription factor NF-kappa B by phosphorylating I kappa B. Proceedings of the National Academy of Sciences. 1994; 91(14):6288–92. https://doi.org/10.1073/pnas.91.14.6288 PMID: 7912826

53. Zamanian-Daryoush M, Mogensen TH, DiDonato JA, Williams BR. NF-κB activation by double-stranded-RNA-activated protein kinase (PKR) is mediated through NF-κB-inducing kinase and IκB kinase. Molecular and cellular biology. 2000; 20(4):1278–90.

54. Pflugheber J, Fredericksen B, Sumpter R Jr, Wang C, Ware F, Sodora DL, et al. Regulation of PKR and IRF-1 during hepatitis C virus RNA replication. Proceedings of the National Academy of Sciences. 2002; 99(7):4650–5. https://doi.org/10.1073/pnas.062055699 PMID: 11904369

55. Sumpter R Jr, Loo Y-M, Foy E, Li K, Yoneyama M, Fujita T, et al. Regulating intracellular antiviral defense and permissiveness to hepatitis C virus RNA replication through a cellular RNA helicase, RIG-I. Journal of virology. 2005; 79(5):2689–99. https://doi.org/10.1128/JVI.79.5.2689-2699.2005 PMID: 15708988

56. Hughes M, Griffin S, Harris M. Domain III of NS5A contributes to both RNA replication and assembly of hepatitis C virus particles. Journal of general virology. 2009; 90(6):1329–34. https://doi.org/10.1099/vir.0.009332-0 PMID: 19264615

57. Targett-Adams P, McLauchlan J. Development and characterization of a transient-replication assay for the genotype 2a hepatitis C virus subgenomic replicon. Journal of general virology. 2005; 86(11):3075–80. https://doi.org/10.1099/vir.0.81334-0 PMID: 16227230

58. Stewart H, Bartlett C, Ross-Thriepland D, Shaw J, Griffin S, Harris M. A novel method for the measurement of hepatitis C virus infectious titres using the IncuCyte ZOOM and its application to antiviral screening. Journal of virological methods. 2015; 218:59–65. https://doi.org/10.1016/j.jviromet.2015.03.009 PMID: 25796989

59. Barba G, Harper F, Harada T, Kohara M, Goulinet S, Matsuura Y, et al. Hepatitis C virus core protein shows a cytoplasmic localization and associates to cellular lipid storage droplets. Proceedings of the National Academy of Sciences. 1997; 94(4):1200–5.

60. Shi ST, Polyak SJ, Tu H, Taylor DR, Gretch DR, Lai MM. Hepatitis C virus NS5A colocalizes with the core protein on lipid droplets and interacts with apolipoproteins. Virology. 2002; 292(2):198–210. https://doi.org/10.1006/viro.2001.1225 PMID: 11878923

61. Peyrou M, Clément S, Maier C, Bourgoin L, Branche E, Conzelmann S, et al. PTEN protein phosphatase activity regulates hepatitis C virus secretion through modulation of cholesterol metabolism. Journal of hepatology. 2013; 59(3):420–6. https://doi.org/10.1016/j.jhep.2013.04.012 PMID: 23623999

62. Vieyres G, Pietschmann T. HCV pit stop at the lipid droplet: Refuel lipids and put on a lipoprotein coat before exit. Cells. 2019; 8(3):233. https://doi.org/10.3390/cells8030233 PMID: 30871009

63. Colpitts CC, Ridewood S, Schneiderman B, Warne J, Tabata K, Ng CF, et al. Hepatitis C virus exploits cyclophilin A to evade PKR. Elife. 2020; 9:e52237. https://doi.org/10.7554/eLife.52237 PMID: 32539931

64. Watanabe T, Ninomiya H, Saitou T, Takanezawa S, Yamamoto S, Imai Y, et al. Therapeutic effects of the PKR inhibitor C16 suppressing tumor proliferation and angiogenesis in hepatocellular carcinoma in vitro and in vivo. Scientific reports. 2020; 10(1):1–9.

65. Cole JL. Activation of PKR: an open and shut case? Trends in biochemical sciences. 2007; 32(2):57–62. https://doi.org/10.1016/j.tibs.2006.12.003 PMID: 17196820

66. Garcia M, Gil J, Ventoso I, Guerra S, Domingo E, Rivas C, et al. Impact of protein kinase PKR in cell biology: from antiviral to antiproliferative action. Microbiology and Molecular Biology Reviews. 2006; 70 (4):1032–60. https://doi.org/10.1128/MMBR.00027-06 PMID: 17158706

67. Targett-Adams P, Boulant S, McLauchlan J. Visualization of double-stranded RNA in cells supporting hepatitis C virus RNA replication. Journal of virology. 2008; 82(5):2182–95. https://doi.org/10.1128/JVI.01565-07 PMID: 18094154

68. Mauger DM, Golden M, Yamane D, Williford S, Lemon SM, Martin DP, et al. Functionally conserved architecture of hepatitis C virus RNA genomes. Proceedings of the National Academy of Sciences. 2015; 112(12):3692–7. https://doi.org/10.1073/pnas.1416266112 PMID: 25775547

69. Kirchhoff S, Koromilas AE, Schaper F, Grashoff M, Sonenberg N, Hauser H. IRF-1 induced cell growth inhibition and interferon induction requires the activity of the protein kinase PKR. Oncogene. 1995; 11 (3):439–45. PMID: 7543195

70. Taniguchi T, Ogasawara K, Takaoka A, Tanaka N. IRF family of transcription factors as regulators of host defense. Annual review of immunology. 2001; 19:623. https://doi.org/10.1146/annurev.immunol.19.1.623 PMID: 11244049

71. Kanazawa N, Kurosaki M, Sakamoto N, Enomoto N, Itsui Y, Yamashiro T, et al. Regulation of hepatitis C virus replication by interferon regulatory factor 1. Journal of Virology. 2004; 78(18):9713–20. https://doi.org/10.1128/JVI.78.18.9713-9720.2004 PMID: 15331704

72. Yamane D, Feng H, Rivera-Serrano EE, Selitsky SR, Hirai-Yuki A, Das A, et al. Basal expression of interferon regulatory factor 1 drives intrinsic hepatocyte resistance to multiple RNA viruses. Nature microbiology. 2019; 4(7):1096–104. https://doi.org/10.1038/s41564-019-0425-6 PMID: 30988429

73. Lindenbach BD, Rice CM. The ins and outs of hepatitis C virus entry and assembly. Nature Reviews Microbiology. 2013; 11(10):688–700. https://doi.org/10.1038/nrmicro3098 PMID: 24018384

74. Lee J-Y, Cortese M, Haselmann U, Tabata K, Romero-Brey I, Funaya C, et al. Spatiotemporal coupling of the hepatitis C virus replication cycle by creating a lipid droplet-proximal membranous replication compartment. Cell reports. 2019; 27(12):3602–17. e5. https://doi.org/10.1016/j.celrep.2019.05.063 PMID: 31216478

75. Mayo CB, Wong CJ, Lopez PE, Lary JW, Cole JL. Activation of PKR by short stem–loop RNAs containing single-stranded arms. Rna. 2016; 22(7):1065–75. https://doi.org/10.1261/rna.053348.115 PMID: 27208315

76. Shimoike T, McKenna SA, Lindhout DA, Puglisi JD. Translational insensitivity to potent activation of PKR by HCV IRES RNA. Antiviral research. 2009; 83(3):228–37. https://doi.org/10.1016/j.antiviral.2009.05.004 PMID: 19467267

77. Toroney R, Nallagatla SR, Boyer JA, Cameron CE, Bevilacqua PC. Regulation of PKR by HCV IRES RNA: importance of domain II and NS5A. Journal of molecular biology. 2010; 400(3):393–412. https://doi.org/10.1016/j.jmb.2010.04.059 PMID: 20447405

78. Hueging K, Weller R, Doepke M, Vieyres G, Todt D, Wölk B, et al. Several human liver cell expressed apolipoproteins complement HCV virus production with varying efficacy conferring differential specific infectivity to released viruses. PloS one. 2015; 10(7):e0134529. https://doi.org/10.1371/journal.pone.0134529 PMID: 26226615

79. Chun J, Riella CV, Chung H, Shah SS, Wang M, Magraner JM, et al. DGAT2 Inhibition Potentiates Lipid Droplet Formation To Reduce Cytotoxicity in APOL1 Kidney Risk Variants. Journal of the American Society of Nephrology. 2022; 33(5):889–907. https://doi.org/10.1681/ASN.2021050723 PMID: 35232775

80. Herker E, Harris C, Hernandez C, Carpentier A, Kaehlcke K, Rosenberg AR, et al. Efficient hepatitis C virus particle formation requires diacylglycerol acyltransferase-1. Nature medicine. 2010; 16(11):1295–8. https://doi.org/10.1038/nm.2238 PMID: 20935628

81. Nakabayashi H, Taketa K, Miyano K, Yamane T, Sato J. Growth of human hepatoma cell lines with differentiated functions in chemically defined medium. Cancer research. 1982; 42(9):3858–63.

82. Blight KJ, McKeating JA, Rice CM. Highly permissive cell lines for subgenomic and genomic hepatitis C virus RNA replication. Journal of virology. 2002; 76(24):13001–14. https://doi.org/10.1128/jvi.76.24.13001-13014.2002 PMID: 12438626

83. Shaw AE, Hughes J, Gu Q, Behdenna A, Singer JB, Dennis T, et al. Fundamental properties of the mammalian innate immune system revealed by multispecies comparison of type I interferon responses. PLoS biology. 2017; 15(12):e2004086. https://doi.org/10.1371/journal.pbio.2004086 PMID: 29253856

84. Macdonald A, Crowder K, Street A, McCormick C, Saksela K, Harris M. The Hepatitis C Virus Non-structural NS5A Protein Inhibits Activating Protein–1 Function by Perturbing Ras-ERK Pathway Signaling. Journal of Biological Chemistry. 2003; 278(20):17775–84. https://doi.org/10.1074/jbc.M210900200 PMID: 12621033

85. Schindelin J, Arganda-Carreras I, Frise E, Kaynig V, Longair M, Pietzsch T, et al. Fiji: an open-source platform for biological-image analysis. Nature methods. 2012; 9(7):676–82. https://doi.org/10.1038/nmeth.2019 PMID: 22743772